2012

Probabilistic Analysis of Offshore Wind Turbine Soil-Structure Interaction

Wystan Carswell
University of Massachusetts Amherst, wcarswel@engin.umass.edu

PROBABILISTIC ANALYSIS OF OFFSHORE WIND TURBINE SOIL-STRUCTURE INTERACTION

A Thesis Presented

by

WYSTAN CARSWELL

Submitted to the Graduate School of the

University of Massachusetts Amherst in partial fulfillment

of the requirements for the

MASTER OF SCIENCE IN CIVIL ENGINEERING

May 2012

Civil and Environmental Engineering

PROBABILISTIC ANALYSIS OF OFFSHORE WIND TURBINE SOIL-STRUCTURE INTERACTION

A Thesis Presented

by

WYSTAN CARSWELL

Approved as to style and content by:

Sanjay R. Arwade, Chair

Don J. DeGroot, Member

Matthew A. Lackner, Member

Richard N. Palmer, Department Head
Civil and Environmental Engineering Department

ACKNOWLEDGMENTS

First and foremost, I would like to thank my family for their endless support. Knowing that they are proud of my accomplishments is one of my biggest inspirations.

I would also like to thank my advisor, Sanjay R. Arwade, for his patience in helping me evolve into the researcher I am today. Additionally, the perspective and commentary provided by my thesis committee members, Matthew A. Lackner and Don J. DeGroot, were invaluable.

I am very appreciative of the education I received as an undergraduate at Lafayette College. The support of my fellow alumni and former professors is a continual motivation for me to work hard and aim high.

Lastly, it should be noted that this project was made possible by generous financial support from the Brack Class of 1960 Graduate Fellowship.

ABSTRACT

PROBABILISTIC ANALYIS OF OFFSHORE WIND TURBINE

SOIL-STRUCTURE INTERACTION

MAY 2012

WYSTAN CARSWELL, B.S., LAFAYETTE COLLEGE

M.S.C.E., UNIVERSITY OF MASSACHUSETTS AMHERST

Directed by: Sanjay R. Arwade

A literature review of current design and analysis methods for offshore wind turbine (OWT) foundations is presented, focusing primarily on the monopile foundation. Laterally loaded monopile foundations are typically designed using the American Petroleum Institute (API) *p-y* method for offshore oil platforms, which presents several issues when extended to OWTs, mostly with respect to the large pile diameters required and the effect of cyclic loading from wind and waves. Although remedies have been proposed, none have been incorporated into current design standards. Foundations must be uniquely designed for each wind farm due to extreme dependence on site characteristics. The uncertainty in soil conditions as well as wind and wave loading is currently treated with a deterministic design procedure, though standards leave the door open for engineers to use a probability-based approach. This thesis uses probabilistic methods to examine the reliability of OWT pile foundations. A static two-dimensional analysis in MATLAB includes the nonlinearity of *p-y* soil spring stiffness, variation in soil properties, sensitivity to pile design parameters and loading conditions. Results are concluded with a natural frequency analysis.

TABLE OF CONTENTS

Page

LIST OF TABLES

Table Page

LIST OF FIGURES

Figure Page

LIST OF VARIABLES

A	Beta distribution parameter
a	Cross-sectional area
A_s, A_c	Variable used for *p-y* curves, (static, cyclic)
B	Beta distribution parameter
b	Pile diameter
$C_{\varphi'\varphi'}$	Covariance
C_1, C_2, C_3	Variables in the API method selected from figures
d	Pile embedment depth
D_R	Relative density
$\boldsymbol{D_s}$	Boundary condition matrix
E	Modulus of elasticity
$E(x)$	Oedemetric modulus (mean stress range)
e, e_{max}, e_{min}	Void ratio (maximum, minimum)
$F_{\varphi'}$	Cumulative distribution function
f_n	Natural frequency (Hz), where *n* is the mode number
g_1, g_2	Safety margins (horizontal pile head displacement, pile head rotation)
H	Horizontally-applied load
I	Moment of inertia
J	Polar moment of inertia
k	Initial modulus of subgrade reaction
$\boldsymbol{K}$	Global stiffness matrix
L_o	Adjusted Pile depth
LR	Linear soil-pile resistance
$\boldsymbol{m}$	Element mass matrix
M	Applied moment

$\boldsymbol{M}$	Global mass matrix
N	Normal (Gaussian) distribution
NLR	Nonlinear soil-pile resistance
p	Pile resistance (force/length)
p_f	Probability of failure
p_u, p_{us}, p_{ud}	Ultimate pile resistance
s_u	Undrained shear strength
u	Horizontal pile head displacement
V	Vertically-applied load
$\boldsymbol{V}$	Displacement column vector
x	Vertical direction
x_k	Vertical distance between soil springs
y	Horizontal direction
y_{50}	Horizontal deflection and 50% of ultimate soil resistance
α	Pile head rotation
β	Reliability index
γ	Total unit weight
δ	Correlation length
ϵ_{50}	50% of maximum principle stress difference
λ	Large diameter effect factor
μ	Mean value
ρ	Mass density
σ	Standard deviation
φ'	Friction Angle
ω	Frequency (rad)

CHAPTER 1

INTRODUCTION AND LITERATURE REVIEW

Offshore wind turbine (OWT) design is a burgeoning area of engineering with roots in the development and research of offshore drilling platforms by the American Petroleum Institute (API) performed in the 1970s. Given recent demands for renewable energy, more attention has been paid to offshore options with the majority of research performed in Europe on OWTs in the North Sea.

Monopiles are the most popular foundation type for OWTs due to the simplicity of load path and definition for wind and wave loading. Laterally loaded monopile foundations are typically designed using the *p-y* method for analysis of the soil-structure interaction, developed by API. The *p-y* method is based on a distributed-spring model, which varies according to soil classification, properties, and location in reference to the water table.

While towers are classified and manufactured typically by turbine rating, foundations must be uniquely designed for each wind farm due to their strong dependence on site characteristics. Unique foundation design is time-consuming with important financial implications. Uncertainty in soil conditions as well as wind and wave loading is currently treated with a deterministic design procedure, though the Det Norske Veritas (DNV) design standard leaves the door open for engineers to use a probability-based approach, which could prevent unnecessary use of materials due to overdesign.

Several problems are inherent in the application of the API *p-y* method for OWTs, as the method was developed for monotonic loading of small-diameter piles. This leads to inaccurate modeling of large diameter OWTs subjected to cyclic loading of wind and waves. Research has been

performed on these discrepancies, but as of yet no adjustments have been incorporated into the design standards.

This thesis uses probabilistic methods to quantify the randomness inherent in wind and wave loading, as well as variability in soil conditions. A two-dimensional monopile model was developed in MATLAB to monitor soil-pile interaction, particularly with reference to pile head rotation.

Under quasi-static loading conditions, the effect of variable soil properties was studied using first order reliability method. Relative density was related to friction angle using the relationship implied by API figures, considering friction angle to be the only varying soil property and all others to be deterministic. Using Monte Carlo simulation to estimate the reliability index (which is related to the probability of failure), the effects of friction angle variance and mean were analyzed for medium-dense to dense sands. The limiting soil property correlation cases of independent variation and perfect correlation are shown to demonstrate the range of potential reliability indices.

After observing how reliability changes with soil properties, a sensitivity analysis was conducted to identify how OWT monopile reliability is effected by pile diameter, wall thickness and embedment depth. This analysis is followed by a brief discussion of large pile diameter effects.

The National Renewable Energy Laboratory (NREL) 5MW Reference Turbine was modeled in MATLAB. By solving the characteristic eigenvalue problem to obtain natural frequency, the effect of soil property variability was examined again.

In conclusion, this thesis describes a summary of findings and recommendations for future work.

1.1 *P-y* Method

The lateral soil-structure behavior of pile foundations is usually characterized using *p-y* curves. Each curve is defined by a unit lateral load (*p*, in units of force per length) and lateral displacement of the pile (*y*) in response to loading (e.g., Figure 1.1). The *p-y* method is based on the Winkler Foundation Theory, which describes soil response as a series of springs. Also called a Distributed Spring model, it was recommended by Bush & Manuel (2009) as well as Bir & Jonkman (2008) as it "most closely represents the true monopile configuration" (Bir & Jonkman, 2008). Winkler Theory assumes semi-infinite pile length as well as constant stiffness of soil and pile (i.e., uniform properties). For pile models such as the one in Figure 1.1, we will consider the difference in depth between each sequential soil spring to be x_k meters.

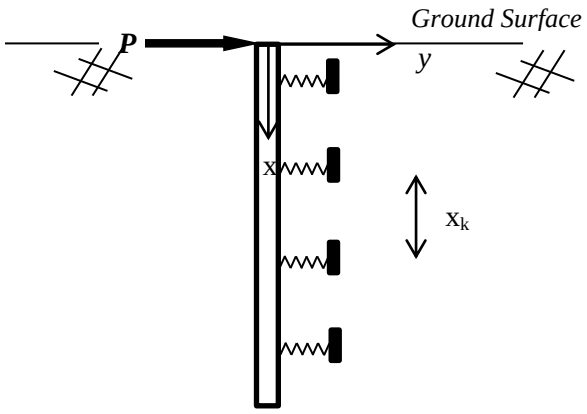

Figure 1.1 Laterally-Loaded Pile

The API method for sand, Matlock's method for soft clay, and Reese et al.'s method for stiff clay use similar soil and pile properties to represent *p-y* soil-structure interaction. For the following *p-y* curve examples, we will consider a reference pile such as the one in Figure 1.1 with the properties listed in Table 1.1 in order to compare the effects of certain soil properties, water table location, and pile diameter variation.

Table 1.1 Properties of Simplified Reference Pile

Symbol	Property	Value
b	Pile Diameter	1 meter
d	Pile Depth	10 meters
x_k	Distance between Soil Springs	2.5 meters

1.1.1 API Method for Cohesionless Soils

The majority of research done on offshore pile foundations has been done by the oil and gas industry for offshore platforms in the 1970s and 1980s (LeBlanc, Houlsby, & Byrne, 2010). The API method for determining *p-y* curves in sand was based on the ultimate resistance (p_u in dimensions of force per unit length) established originally by Reese et al. (1975) and then checked by O'Neill and Murchison (LeBlanc, Houlsby, & Byrne, 2010). The API method, described in API RP2A, is fundamentally influenced by the angle of internal friction φ', total soil unit weight γ, and pile diameter b, where

$$p = Ap_u \tanh\left(\frac{kx}{Ap_u} y\right) \tag{1.1}$$

where A is either A_s or A_c:

$$A_s = \left(3.0 - 0.8\frac{x}{b}\right) \geq 0.9 \text{ for static loading}$$
$$A_c = 0.9 \text{ for cyclic loading} \tag{1.2}$$

and the initial modulus of subgrade k is obtained from Figure 1.2 as a function of φ' and water table location.

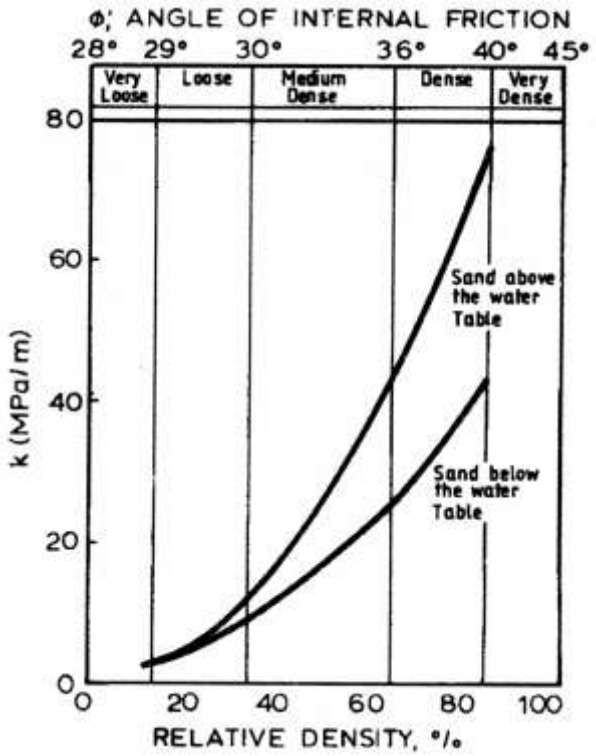

Figure 1.2 Initial Modulus of Subgrade *k* as a Function of Friction Angle (DNV, 2009)

The ultimate soil resistance at a selected depth, p_u, is given by

$$p_u = \min(p_{us}, p_{ud}) \tag{1.3}$$

$$p_{us} = (C_1 x + C_2 b)\gamma x \tag{1.4}$$

$$p_{ud} = C_3 b \gamma x \tag{1.5}$$

where p_{us} is the ultimate soil resistance at shallower depths, p_{ud} is the ultimate soil resistance at deeper depths, and C_1 and C_2 are coefficients determined as a function of φ' from Figure 1.3.

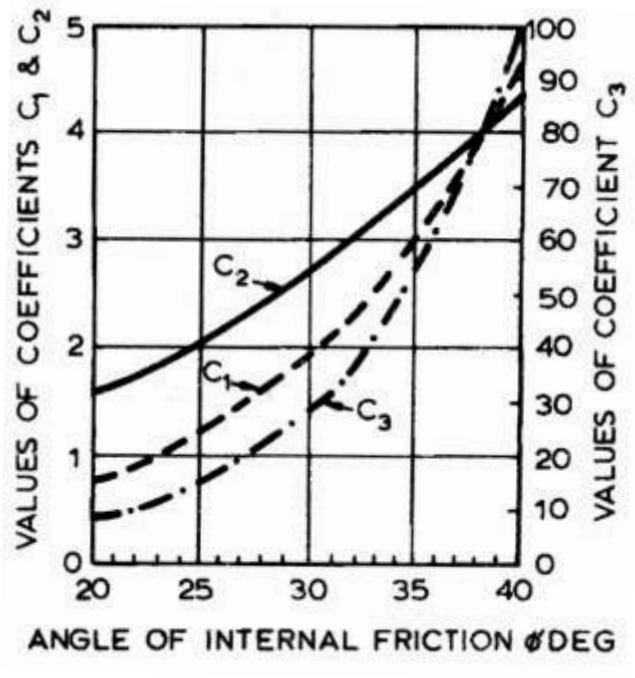

Figure 1.3 Coefficients as Function of Friction Angle (DNV, 2009)

Using the four-spring reference model (Fig. 1.1, Table 1.1), the soil properties from Table 1.2, and assuming the water table is located below the pile, the API method yields four curves – one for each spring.

Table 1.2 Reference Properties for Sand

Symbol	Property	Value/Description
φ'	Angle of Internal Friction	35°
γ	Total Soil Unit Weight	17 kN/m^3
k	Initial Modulus of Subgrade Reaction	38 MPa

Since the p values are in units of force per unit length, they are multiplied by the tributary length along the pile, x_k, in order to create a curve of lateral force (kN) versus displacement (m) such as in Figure 1.4.

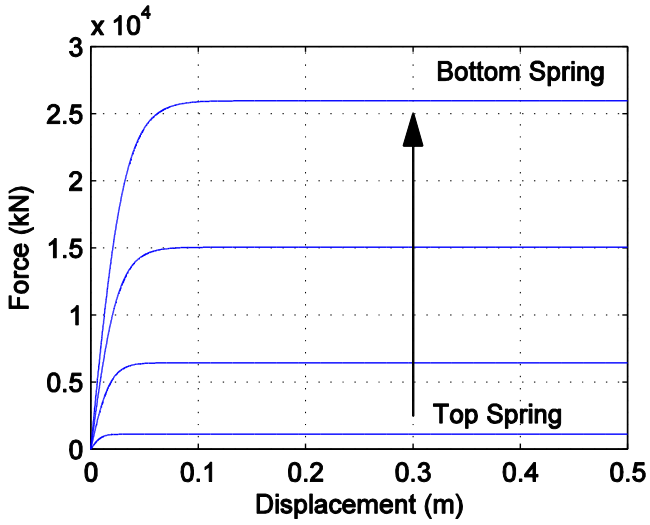

Figure 1.4 Force-Displacement Curves

Figure 1.4 illustrates clearly that the initial stiffness and soil strength increases with depth. It can be seen by visual inspection of Equations 1.4 and 1.5 that increasing φ', γ, or b will also cause the strength of the soil to increase. Using the force-displacement curve representing the bottom pile spring from Figure 1.4 as a baseline for comparison, we can see how the behavior of *p-y* curves is affected by adjusting φ', γ, or b to approximately $\pm$15% of the control variables.

In the case of Figure 1.5, we note the difference in ultimate strength when φ' is equal to 30°, 35°, and 40° - classified by friction angle alone, these sands could be respectively considered loose sand, medium sand, and dense sand (Van Nostrand Reinhold, 2002). When φ' is increased from 35° to 40°, the basic shape of the force-displacement curve remains unchanged but the soil-pile resistance increases by approximately $1x10^4$ kN. Decreasing φ' from 35° to 30° results in a similar decrease in soil-pile resistance but also "softer" curve (decreased initial stiffness).

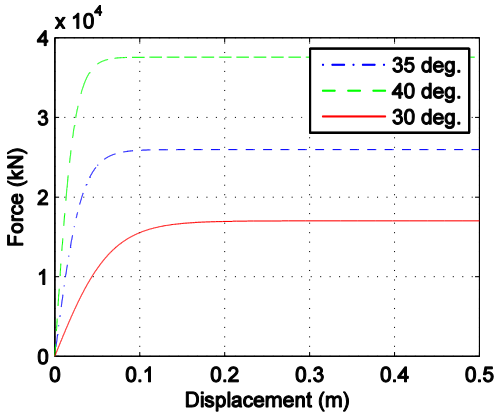

Figure 1.5. *P-y* Behavior with Respect to Internal Friction Angle

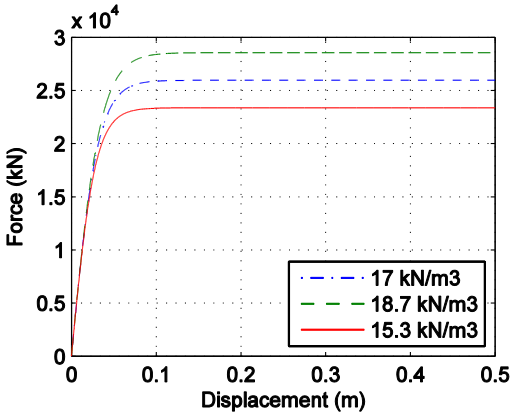

Figure 1.6. *P-y* Behavior with Respect to Unit Weight

Altering the total unit weight, γ, of the soil has much less of an effect than changing the friction angle. Figure 1.6 shows that a 15% change in total unit weight results in a soil-pile resistance difference of $0.25 \text{x} 10^4$ kN.

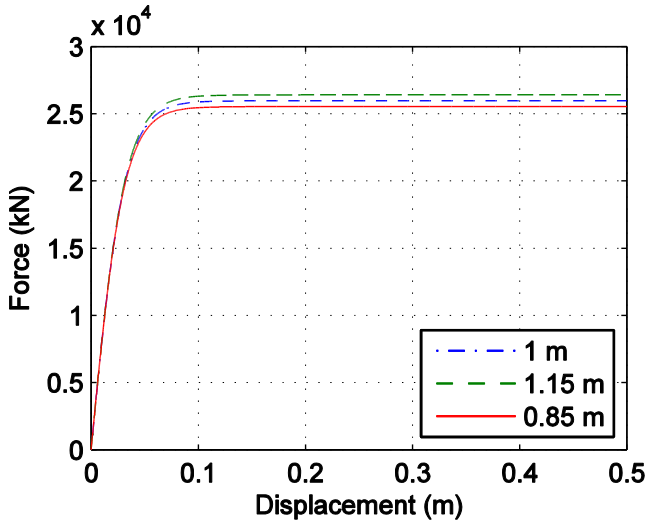

Figure 1.7. *P-y* Behavior with Respect to Pile Diameter

Soil-pile resistance differences resulting from a 15% change in pile diameter demonstrated in Figure 1.7 are very minimal.

Due to the fact that k, C_1, C_2, and C_3 are all a function of the friction angle φ', *p-y* curves are far more sensitive to change in φ' than total unit weight, γ. It should also be noted that the initial stiffness is not affected by changes in unit weight or pile diameter, as the derivate of the *p-y* curve, $\frac{dp}{dy}$, is purely reliant on depth and modulus k.

If we compare the same sand properties at a position below the water table (reducing the value of k found in Figure 1.2), we note that the shape of the curve changes but the ultimate strength remains the same. Sand above the water table reaches ultimate soil-pile resistance sooner than sand below the water table (see Figure 1.8).

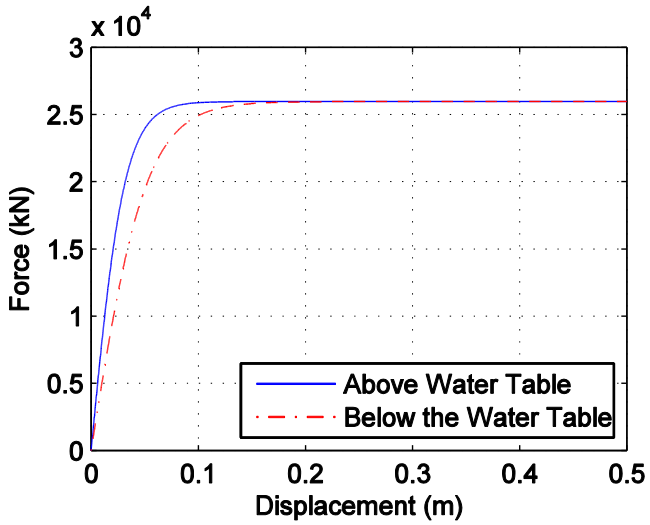

Figure 1.8. *P-y* Behavior with Respect to Water Table Location

We can conclude from the figures above that the properties of the soil reacting to a laterally loaded pile have a more profound effect on the ultimate strength of the foundation than pile diameter.

It should be noted that generally friction angle increases with unit weight, and the two quantities are not independent of one another (Day, 2000). Thus, the cases shown above should be considered only for qualitative purposes.

1.1.2 P-y Curves for Cohesive Soils

Cohesive soils, or clays, behave differently under lateral loading than cohesionless soils. Cohesionless soils below the ground water table require a reduced initial modulus of subgrade; for cohesive soils, an entirely different set of equations are required to illustrate *p-y* behavior.

1.1.2.1 Soft Clay Below the Water Table

The response of soft clay below the water table to short-term lateral static loading is a function of the undrained shear strength s_u and the unit weight of the soil developed by Matlock (1970), where

$$\frac{p}{p_u} = 0.5\left(\frac{y}{y_{50}}\right)^{\frac{1}{3}} \tag{1.6}$$

where p is the soil resistance per unit length of pile, y is the lateral deflection from p, and y_{50} is the deflection at 50% of the ultimate soil resistance strength, p_u. This value is given by the equation

$$y_{50} = 2.5\varepsilon_{50}b \tag{1.7}$$

where b is the pile diameter and ε_{50} is the strain corresponding to 50% of the maximum principal stress difference, or one-half of the maximum stress in laboratory undrained compression tests of undisturbed samples.

The ultimate soil resistance p_u is given by

$$p_u = \min(p_{us}, p_{ud}) \tag{1.8}$$

$$p_u = \left[3 + \frac{\gamma'}{s_u}x + \frac{J}{b}x\right] s_u b \tag{1.9}$$

$$p_u = 9 s_u b \tag{1.10}$$

where γ' is the average effective unit weight from ground surface to the soil spring, x is the depth to the soil spring, and s_u is the undrained shear strength at depth x. The variable J is typically 0.5.

Using the reference four-spring model, force-displacement curves from the properties listed in Table 1.3 would appear as in Figure 1.9.

Table 1.3. Reference Properties for Soft Clay

Property	Value
γ'	6 kN/m^3
s_u	20 kN/m^3
J	0.5

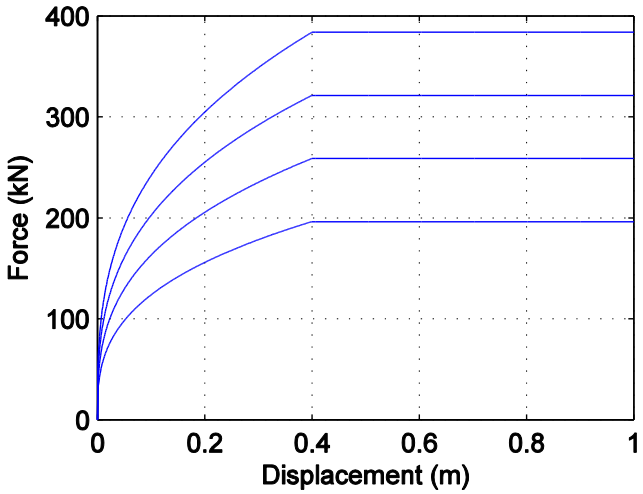

Figure 1.9. Force-Displacement Curves for Soft Clay

1.1.2.2 Stiff Clay Above the Water Table

The Reese, Cox and Koop (1975) *p-y* curve development procedure for stiff clay above the water table is based on lateral load tests similar to Matlock's, differing from soft clay only in exponent: ¼ instead of ⅓ (see Equation 1.11).

$$\frac{p}{p_u} = 0.5\left(\frac{y}{y_{50}}\right)^{\frac{1}{4}} \tag{1.11}$$

However, the ultimate strength displacement limit is twice that of soft clay: $p = p_u$ for $y > 16y_{50}$.

Table 1.4. Reference Properties for Stiff Clay

Property	Value
γ	19 kN/m^3
s_u	100 kN/m^3
J	0.5

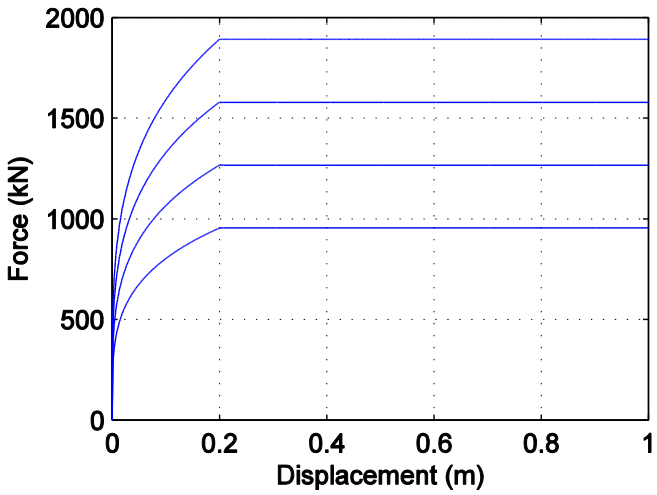

Figure 1.10. Force-Displacement Curves for Stiff Clay

For the values in Table 1.4, the stiff clay force-displacement curves would appear as in Figure 1.10. If we compare both soft and stiff clays (as in Figure 1.11), we note that stiff clay can provide significantly more soil-pile resistance than the soft clay.

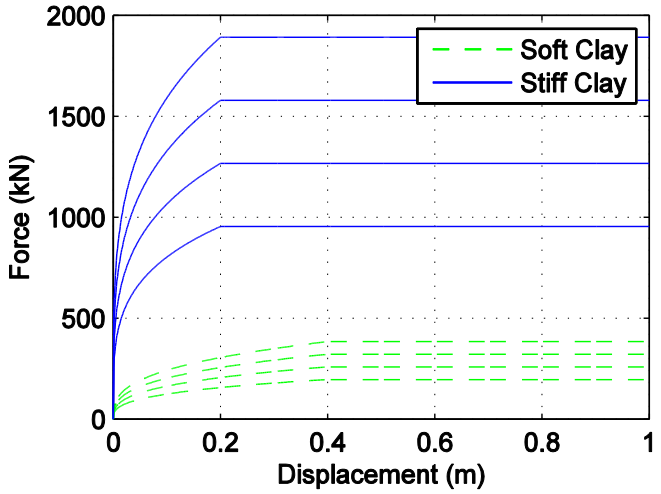

Figure 1.11 Comparison of Soft and Stiff Clay Force-Displacement Curves

As seen in Figure 1.12, this sample of stiff clay cannot provide as much soil-pile resistance as sand – in this case, the lowest spring is weaker by a factor of 5. However, for the reference values chosen, the soil resistance difference from the top spring to the bottom spring is much smaller for stiff clay than sand.

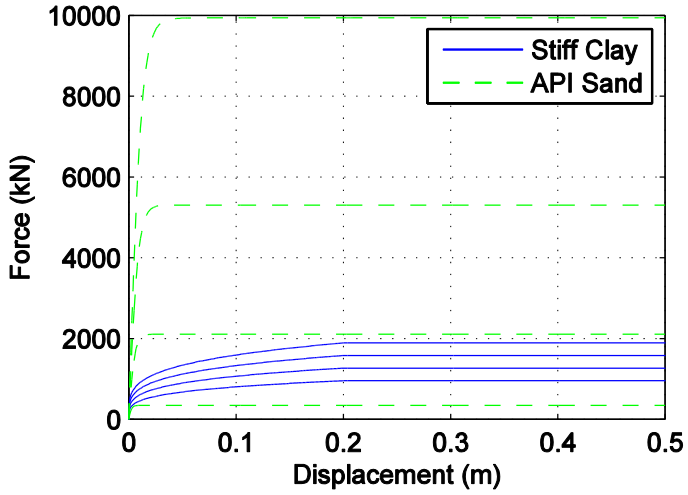

Figure 1.12 Comparison of Stiff Clay and Sand

1.1.2.3 Stiff Clay Below the Water Table

The method for developing *p-y* curves for stiff clay in the presence of free water is significantly different than stiff clay above the water table. The curve is segmented into several different sections which are characterized by

$$p_u = \min(p_{ct}, p_{cd}) \tag{1.12}$$

$$p_{ct} = 2s_u b + \gamma' bx + 2.83 s_u x \tag{1.13}$$

$$p_{cd} = 11 s_u b \tag{1.14}$$

Where s_u is the average undrained shear strength over the depth x, b is the pile diameter, and γ' is the submerged, or effective soil unit weight. Depending on the normalized depth (i.e., depth to the

soil spring divided by the total pile length), a value of A_s is selected from Figure 1.13 (*B* represents the coefficient required for the cyclic process, not described here).

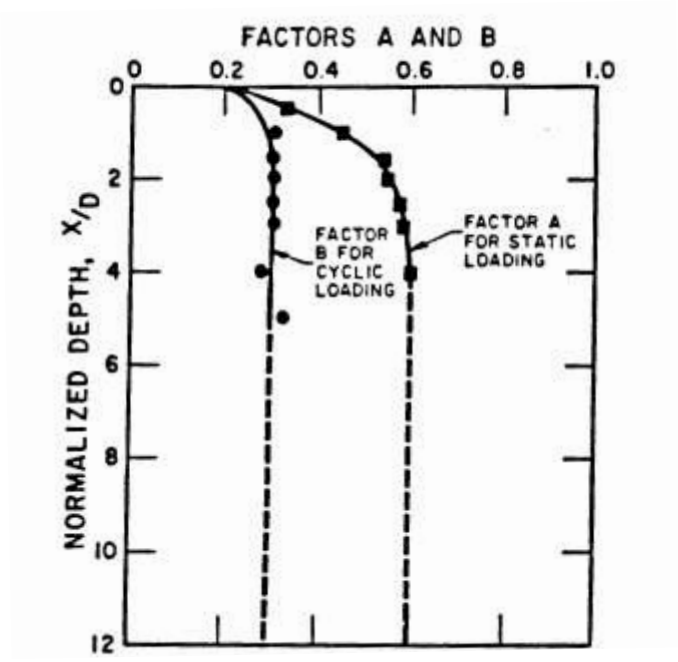

Figure 1.13 Empirical Factors for Ultimate Resistance (Kramer, 1988)

The initial straight-line portion of the *p-y* curve is described by

$$p = (kx)y \tag{1.15}$$

where *k* is obtained from Table 1.5.

Table 1.5 Representative Values of *k* for Stiff Clays (LPILE Plus 5.0, 2005)

Average Unconsolidated Undrained Shear Strength			
s_u (kPa)	50-100	100-200	300-400
k (static, MN/m^3)	135	270	540

The next portion of the curve begins at the intersection of the straight line and the parabolic curve

$$p = 0.5p_u\left(\frac{y}{y_{50}}\right)^{\frac{1}{2}} \tag{1.16}$$

where

$$y_{50} = \varepsilon_{50}b \tag{1.17}$$

The third portion of the *p-y* curve begins when *y* is equal to $A_s y_{50}$ and extends to *y* equal to $6A_s y_{50}$.

$$p = 0.5p_u\left(\frac{y}{y_{50}}\right)^{\frac{1}{2}} - 0.055p_u\left(\frac{y - A_s y_{50}}{A_s y_{50}}\right)^{1.25} \tag{1.18}$$

From *y* equals $6A_s y_{50}$ to *y* equals $18A_s y_{50}$,

$$p = 0.5p_u\sqrt{6A_s} - 0.411p_u - \frac{0.0625}{y_{50}}p_u(y - 6A_s y_{50}) \tag{1.19}$$

After $18A_s y_{50}$,

$$p = 0.5p_u\sqrt{6A_s} - 0.411p_u - 0.75p_u A_s \tag{1.20}$$

Given the same characteristics described in Table 1.4 for stiff clay above the water table, the *p-y* curves for the simple four-spring model appear as in Figure 1.14.

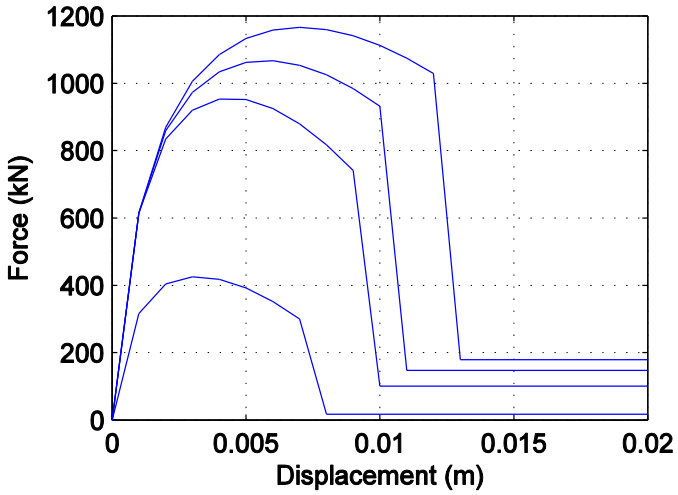

Figure 1.14 P-y Curves for Stiff Clay Below Ground Water Table

Note that the range of displacement shown is only from 0 to 0.02 m.

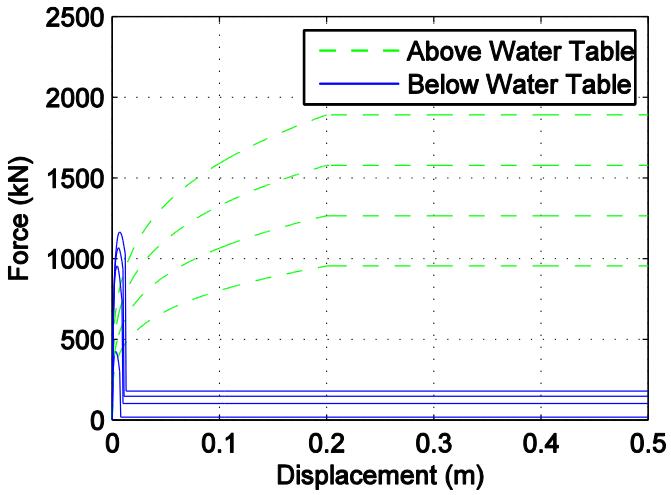

Figure 1.15 Saturated and Unsaturated Comparison of Stiff Clay *p-y* Behavior

When stiff clay becomes saturated, the difference in *p-y* behavior is very obvious (see Figure 1.15). While the resistance of the pile for saturated stiff clay peaks earlier than unsaturated stiff clay, pile resistance drops almost immediately afterwards. The ultimate soil-pile resistance for the bottom spring in unsaturated stiff clay, in this instance, is greater by a factor of approximately 1.5 and is sustained after a displacement of 0.2 m.

1.2 Current Design Practices

Offshore wind turbines (OWTs) are comprised of a nacelle (hub that houses the mechanical components, including rotor), rotor blades, tapering transition tower section, tower, and foundation (see Fig. 1.16). The towers are usually made in 20-30 m long sections (limited by transportation) of rolled and welded steel plate, while the rotor blades are made of fiberglass (Malhotra, 2010).

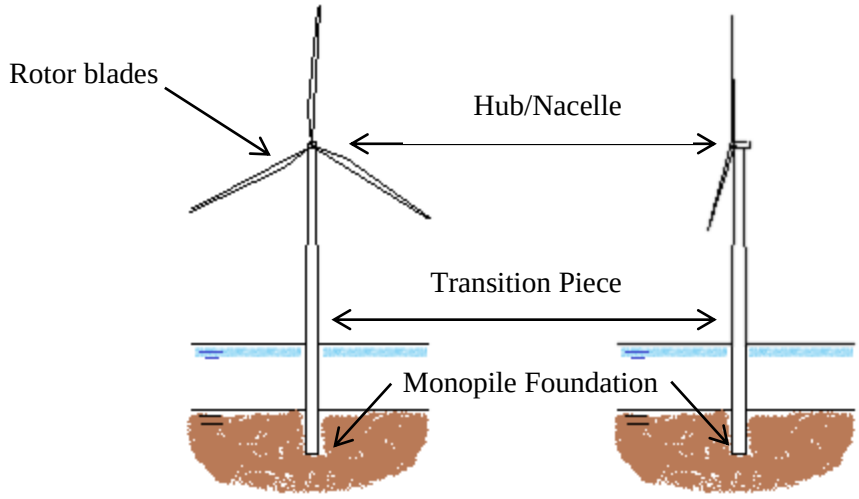

Figure 1.16 Basic Offshore Wind Turbine Diagram

Increasing renewable energy production demands that OWTs in the United States need to be 5MW or greater for economic feasibility, requiring wind farms to move out to depths of 30-50 m where wind speeds are higher and more uniform. As of 2008 however, 40% of OWTs were rated at 1.5MW or higher with the typical range being 2.0 to 3.6MW (Bolinger & Wiser, 2008), (Department of Energy, 2010).

While the tower designs are specified by maximum power output, foundations are entirely site specific due to dependency on environmental and soil factors. These factors include scour, water depth, marine growth, sea ice, wind, wave, and soil profile data.

1.2.1 **Foundation Types**

Offshore wind turbine foundations are chosen mostly by water depth, as hydrodynamic loading generally dominates design. Depths are separated into the categories of deep, shallow, and transitional (see Fig.1.17).

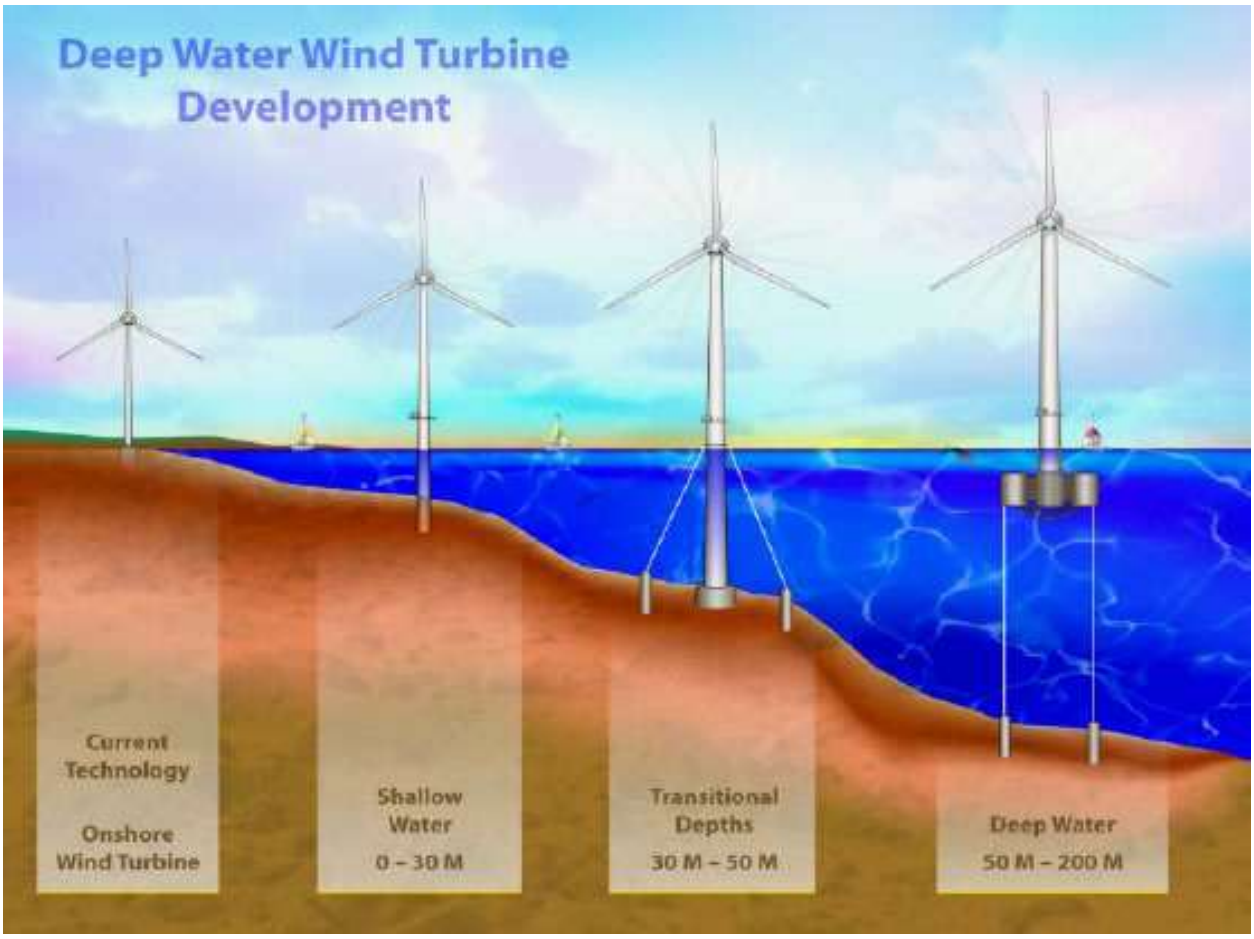

Figure 1.17. Types of Support Structures and their Applicable Water Depths (NREL, 2009)

The large mass and inertia of the gravity foundation (see Figure 1.18, center) have been found attractive for the rough conditions of the North Sea, given that installation does not require specialized vessels (Stancich, 2010). However they are limited to feasible installation depths of less than 20 m and require extensive site preparation (Malhotra, 2010). Minimizing structural dead weight for gravity foundations (while also providing sufficient dead weight) is challenging (Thomsen, Forsberg, & Bittner, 2007).

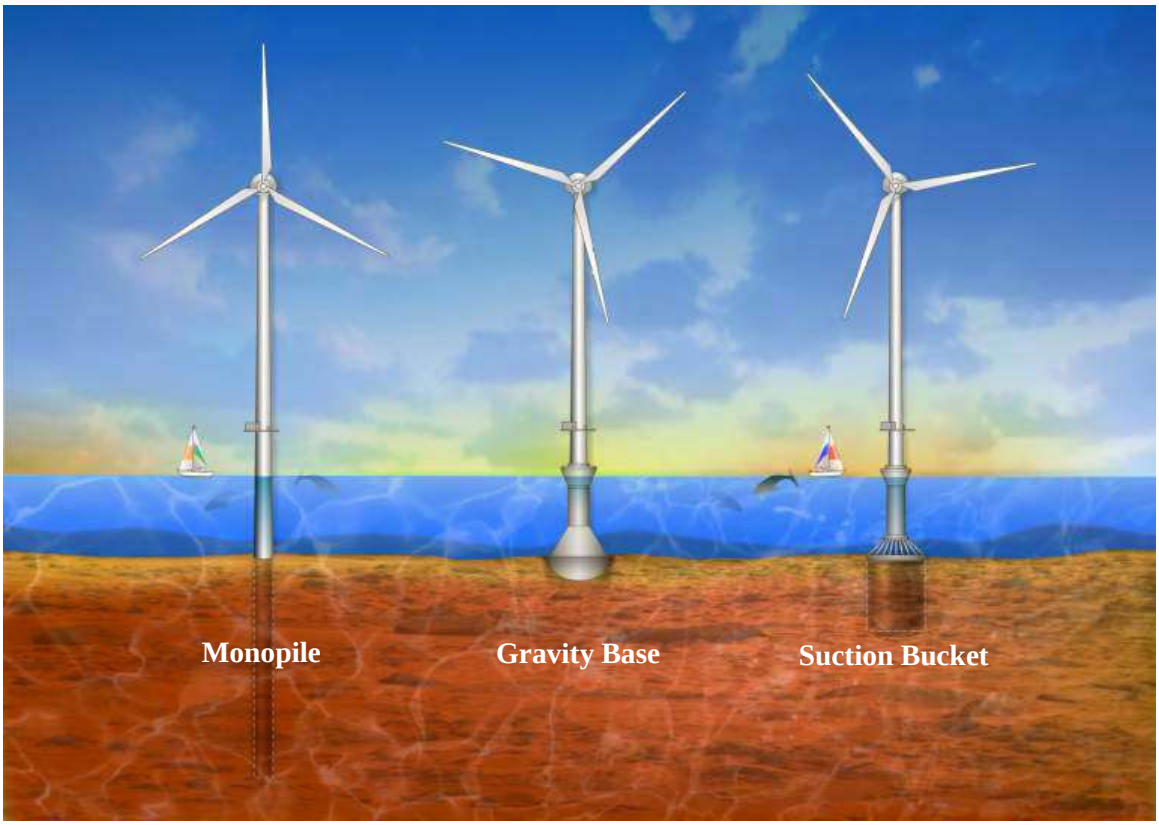

Figure 1.18. Monopile, Gravity Base, and Suction Bucket Foundations (Musial & Ram, September 2010)

Suction caissons (or buckets, see Figure 1.18 right) are time-consuming and labor-intensive to install as well as having limited installation depths (Malhotra, 2010). Suction caissons perform optimally in soft clay situations where a seal can form around the caisson during suction in the installation process; any soil material that is prone to fissures can inhibit the formation of a seal and therefore is unsuitable (Houlsby & Byrne, 2005).

The monopile design (see Figure 1.18, left) is simple, providing a direct load path from the tower to the soil and clearly defined loading from wind and waves. While installation can be noisy, monopiles are otherwise considered to have the least environmental impact on marine ecologies due to their unobtrusive geometry – also an advantage regarding damage risks in the event of ship collision (Abdel-Rahman & Achmus, 2005). There is some disagreement in reference to the

depths at which a monopile is appropriate, but it is the overwhelmingly popular choice for OWTs and will thus be the focus of this study. It is generally agreed that monopiles are feasible for depths up to 30m, though some would say even up to 40 or 50 m (Lesny & Hinz, 2007; Malhotra, 2010).

The challenge of installation dictates the depths to which monopiles are feasible, as the jack-up installation barges currently used have a maximum water depth of 25-30 m; however, new techniques have allowed installation up to 45 m (Musial & Ram, September 2010). For anything in excess of 45 m, innovation in floating platform foundations may be the answer (Musial & Ram, September 2010).

Multi-pile substructures (such as tripods) are typically used for depths that exceed the practical limits of monopiles. Tripod foundations are considered to be the "most promising" foundation for depths greater than 30 m, but monopiles may be an alternative (Abdel-Rahman & Achmus, 2005).

1.2.2 **Typical Dimensions**

A typical monopile foundation has a 4-m diameter and penetration depth up to 18 m, with a length/diameter ratio of approximately 5 (LeBlanc, Houlsby, & Byrne, 2010). However, in order to support the loading incurred by a 5MW OWT, diameters can be as large as 8 m with wall thicknesses up to 60 mm. Wall thickness to diameter ratios of a typical monopile are typically 1:50 to 1:80 (LeBlanc, Houlsby, & Byrne, 2010), (de Vries & Krolis, 2004).

Despite vast offshore wind resources, there are no offshore wind turbines in the United States to date due primarily to cost, but also regulatory and permitting issues (Musial & Ram, September 2010). However, the National Renewable Energy Laboratory (NREL), a research laboratory of the U.S. Department of Energy, has sponsored several studies on OWTs. In order to "support

concept studies aimed at assessing offshore wind technology", the NREL 5MW baseline wind turbine was created from a compilation of several manufactured models (Jonkman, Butterfield, Musial, & Scott, 2009). This study will use the specifications of the NREL 5MW baseline OWT with properties listed in Table 1.6.

Table 1.6 NREL 5MW Offshore Wind Turbine Properties (Jonkman, Butterfield, Musial, & Scott, 2009)

Property	Value
Rotor, Hub Diameter	126 m, 3 m
Hub Height	90 m
Tower Base Diameter & Wall Thickness	6 m, 0.027 m
Tower Top Diameter & Wall Thickness	3.87 m, 0.019 m
Young's and Shear Modulus of Steel	210 GPa, 80.8 GPa
Cut-In, Rated, Cut-Out Wind Speed	3 m/s, 11.4 m/s, 25 m/s
Cut-In, Rated Rotor Speed	6.9 rpm, 12.1 rpm
Rated Tip Speed	80 m/s
Overhang, Shaft Tilt, Precone	5 m, 5°, 2.5°
Rotor Mass	110,000 kg
Nacelle Mass	240,000 kg
Tower Mass	347,460 kg

It is assumed that the tower tapers linearly from the base properties to the top properties (Jonkman, Butterfield, Musial, & Scott, 2009).

1.2.3 **Design Standards**

Design standards are currently region-based. Both Germany and Denmark have national design standards for OWTs, but the majority of OWT foundation design relies on the American Petroleum Institute Recommended Practice 2A (API RP 2A), International Design Standard for

Offshore Wind Turbines (IEC 61400-3), Det Norske Veritas (DNV), and Germanischer Lloyd (GL) design documents. As of December 2010, the American Bureau of Shipping (ABS) released a guide for building and classing of offshore wind turbine installations, which is based primarily on API standards and IEC 61400-3.

Unlike the other design standards, API RP 2A was compiled in reference to fixed offshore platforms as opposed to offshore wind turbines. As such, it includes a higher level of detail in design due to life safety concerns and the delicacy of offshore drilling. However, the API *p-y* method is used by all of the design standards for designing monopile foundations.

The design standards typically cite a return period of 50 years in reference to extreme wind and wave loading, though ABS uses a 100-year return period. These return periods are intended to designate the design lifetime of the structure, though the IEC 61400-3 uses a 50-year return period but states a design lifetime of 20 years (IEC 61400-3, 2009).

While the primary design methods are deterministic with partial safety factors (ranging from 1.0 to 1.5, applied to both loads and materials) for most design standards, some standards also allow for the use of probabilistic methods. The DNV (2009) standard allows for calibrating deterministic design methods or for special designs with which there is limited experience, the GL (2005) standard for the designer to use probabilistic methods of analysis with consultation, and ABS (2010) for obtaining environmental condition values.

1.2.4 **Limit States**

This thesis will focus on the pile foundation of the OWT which is designed to support the sustained weight of the hub, nacelle, tower and transition piece. In addition to withstanding these deterministic gravity loads, the foundation must resist stochastic loading from wind and waves (see Fig 1.19). While axial loading is taken into consideration, hydrodynamic lateral loading is

generally governing (de Vries & Krolis, 2004). The tower is designed for extreme load cases initially, and then operational load cases are checked (Lesny & Hinz, 2007).

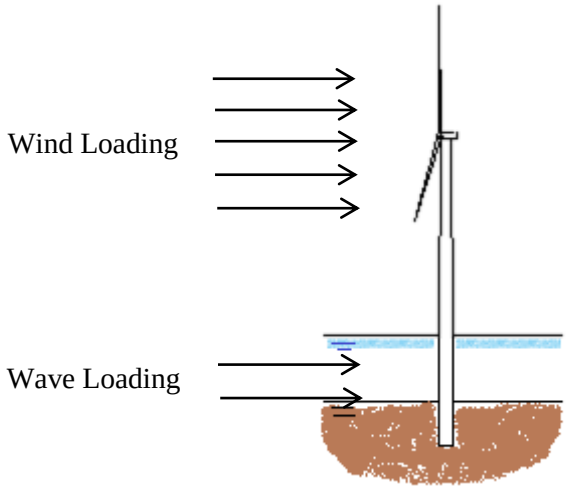

Figure 1.19 Offshore Wind Turbine Subjected to Lateral Loading

As considering the extreme state of both wind speed and wave height simultaneously is considered too conservative, extreme wind gusts are taken into account with reduced wave heights; a process very reminiscent of traditional load and resistance factor design where extreme events are not considered to occur simultaneously (Quarton, 2005). The design cases considered are when wind and waves are aligned (co-directional) and when acting from a single worst case direction (uni-directional) (Quarton, 2005).

Design standards define limit state levels in different ways, though the most commonly referenced are the Serviceability Limit State (SLS) and Ultimate Limit State (ULS), where SLS is defined by the DNV as “deflections that may prevent intended operation of equipment” and ULS refers to structural failure (DNV, 2009).

The main structural limit states considered depend on resistance to cyclic/dynamic loading and mudline rotation. Cyclic loading from wind, waves, and mechanical vibrations are a major factor

in design considerations. Mechanical vibrations are classified into two main frequency intervals referred to as 1P and 3P, for the excitation caused by the rotation of one rotor blade and the combination of all three rotor blades, respectively (see Fig. 1.20 for the Vestas V90 3.0 MW wind turbine situated in the North Sea).

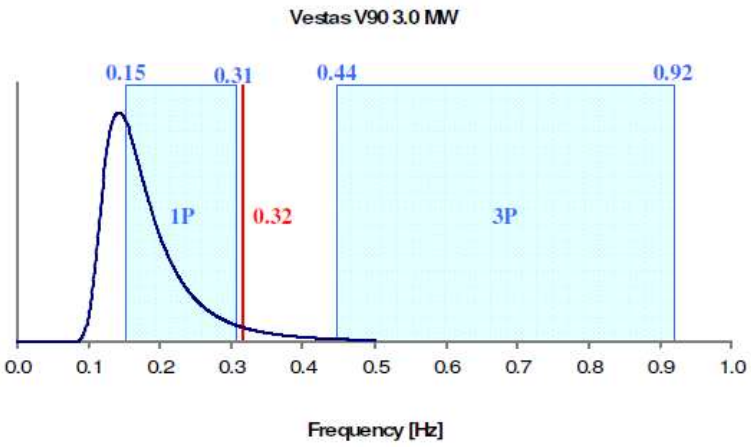

Figure 1.20 Depiction of Natural and Excitation Frequencies (de Vries & Krolis, 2004)

After the natural period for the tower has been selected to avoid resonance, the diameter and wall thickness of the tower are designed to withstand environmental factors (such as marine growth and ice) as well as standard loading. After the general properties are selected to prevent buckling, sufficient embedment depth of the monopile foundation is required. Embedment depths to prevent foundation failure are defined by the equation

$$d = \lambda * L_o \; with \; L_o = \sqrt[5]{\frac{EJ * x}{b * k(x)}} \tag{1.21}$$

where λ typically varies between 4 and 5, J is the polar moment of inertia, b is the diameter of the pile, and k is the initial modulus of subgrade and

$$E(x) = \left(\frac{x}{L}\right)^{0.5} * E_{max} \quad \textbf{(1.22)}$$

where *E(x)* is the oedemetric modulus (mean stress range) which, for Essen Sand, is 50-80 MN/m^2 (Lesny, Paikowsky, & Gurbuz, 2007).

After sufficient embedment depth is achieved, mudline rotation must be minimized in order to keep the wind turbine within efficient operational levels. Wiemann, Lesny & Richwien (2004) state that the pile head rotation cannot exceed 0.7° and still be considered a rigid foundation, which is a standard design assumption. In addition to this, the GL standard used by de Vries & Krolis (2004) restricted horizontal displacement at the mudline to 0.2 m.

1.3 Uncertainty in Offshore Wind Turbine Design

Uncertainty in OWT design is currently treated by using conservative deterministic methods. Since the random loading of wind and waves dominate design, conservatism leads to larger (and therefore more expensive) towers and foundations.

Towers are designed for particular return periods for both the wind and waves according to metocean data, and the towers are assumed to have a lifetime equivalent to these return periods.

In addition to the uncertainty in wind and wave loading, soil is a large source of uncertainty since it is not a homogeneous material. Site characterization often calls for at least one boring in the installation area, with more specific site tests per requirement of the applicable design standard, providing designers with the general soil profile of the wind farm site. Not only is the soil variable, but the measurement methods utilized are also uncertain.

In an assessment on the Platform Cognac (a deep-water platform installed in 1978 according to API standards), it was determined that the largest source of bias occurred in the foundation stiffness, from estimations of clay strength and stiffness (Gur, Choi, Abadie, & Barrios, 2009).

1.4 *P-y* Curves for Large Diameter Piles

The API method for determining *p-y* curves was based on testing of slender piles of 0.6-m diameter and confirmed for pile diameters up to 2 m (Wiemann, Lesny, & Richwien, 2004). Despite its limitations, monopiles with diameters up to 4.5 m have been installed using this method. Studies show that the API method greatly overestimates the stiffness at large depths for large-diameter piles, resulting in insufficient embedment lengths for the piles and negates the design assumption that the OWT tower is rigidly affixed in the soil (Lesny & Wiemann, 2005), (Krolis, van der Tempel, & de Vries, 2007). This overestimation in soil strength can lead to pile deflection underestimation of up to 120% (Lesny, Paikowsky, & Gurbuz, 2007).

For significant pile deformations, shear stresses are induced around the perimeter of the foundation which the API *p-y* method does not take into account for large diameter piles (Lesny, Paikowsky, & Gurbuz, 2007).

Lesny & Wiemann (2006) suggest a modification for large diameter open pipes, but it has not yet been adopted by design standards.

1.5 Cyclic Loading in Offshore Wind Turbine Design

Cyclic loading of OWTs impacts both the tower and foundation. The structural integrity of the tower can be compromised by way of fatigue or damage caused by resonance, with the most challenging aspect of modeling being the randomness of wind and wave loading.

Unlike structural components, the modeling of cyclic effects on soil requires the incorporation of randomness in both the loading and the material. Cyclic loading causes the soil surrounding the monopile foundation to develop plastic strains. As the life of the OWT proceeds, the stiffness of the foundation decreases. This decrease in stiffness increases deflection and rotation, hampering the efficiency of the turbine operation and increasing the possibility of failure (Lesny & Hinz, 2007).

LeBlanc, Houlsby, & Byrne (2010) performed long-term cyclic studies on 80.0 mm piles in sand. According to their results, stiffness increased with the number of cycles independent of relative density for undrained piles; however, further work is necessary to examine how applicable these results are for larger piles (LeBlanc, Houlsby, & Byrne, 2010).

Wind is modeled as one-way cyclic loading (see Figure 1.21), which is more conservative in regards to soil degradation than two-way cyclic loading (Krolis, van der Tempel, & de Vries, 2007). The results of small-scale testing by LeBlanc, Houlsby, & Byrne (2010) revealed that the difference between accumulated rotation from one-way cyclic loading can differ from two-way loading by as much as a factor of four.

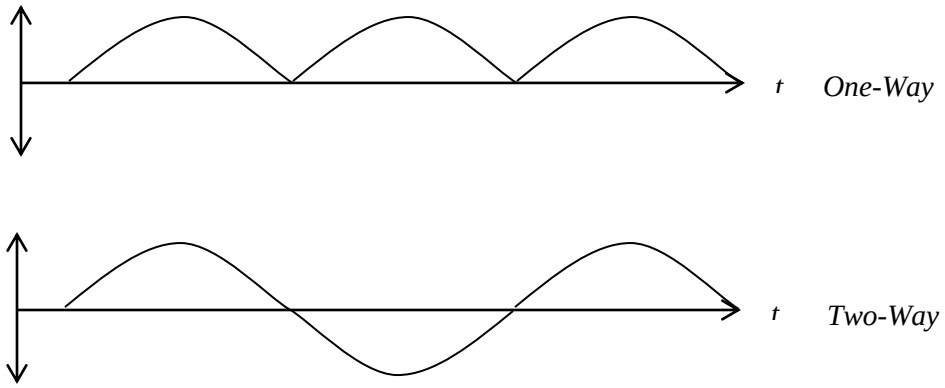

Figure 1.21 Depiction of One-Way and Two-Way Cyclic Loading

Without derivation or explanation, the API method applies a factor of 0.9 to *p-y* curves for cyclic conditions (Krolis, van der Tempel, & de Vries, 2007). Though evidently it has theory behind it, the factor is highly empirical (LeBlanc, Houlsby, & Byrne, 2010).

The Deterioration of Static *p-y* Curve (DSPY) Method proposed by Long & Vanneste (1994) takes into account the type, number of cycles, and magnitude of cyclic loading as well as the method of pile installation, soil density, and whether the pile has been precycled or not (Krolis, van der Tempel, & de Vries, 2007). The DSPY Method incorporates a linearly increasing lateral (horizontal) subgrade modulus *k* with depth for each individual number of cycles in which the spring stiffness decreases (Krolis, van der Tempel, & de Vries, 2007).

Testing for the DSPY method was performed on long, flexible piles for fewer than 50 cycles of loading and so as such is not yet approved for high cyclic loading of large-diameter piles (Krolis, van der Tempel, & de Vries, 2007), (LeBlanc, Houlsby, & Byrne, 2010).

1.6 Conclusions

This literature review provides a general overview of OWT foundations and design. Various foundation options are being considered by the engineering community, but up to this point the monopile foundation has proved most popular. While an enormous amount of research is currently being performed, the limitations of current monopile design methodologies are apparent: the API *p-y* method is based on research performed for small piles supporting offshore platforms. Significant issues arise when the empirical relationships derived from this research are extrapolated for the design of OWT monopile foundations, particularly for pile diameters larger than 2 m. Design standards do not currently include adjustments for large diameter piles, despite the fact that finite element models have shown that the API *p-y* method overestimates soil-pile resistance.

While the API *p-y* method suggests a decrease in soil-pile resistance for piles under cyclic loading, small-scale research by LeBlanc, Houlsby, & Byrne (2010) showed that pile stiffness increased with the number of cycles, independent of relative density. The DSPY method, proposed by Long & Vanneste (1994), has been suggested to more closely replicate cyclic behavior of laterally loaded piles. Before applied to OWT large diameter conditions, more research is required to validate the method and results.

As renewable energy gains global interest, research in offshore wind becomes more critical. The pressure to supply energy independent of fossil fuels increases, and with it the demand for economically feasible OWT designs.

The following chapters explore the application of reliability to the design of OWT pile foundations in cohesionless soils, examining the effects of soil variation, load variation, and large diameters. Lastly, a natural frequency analysis will explore the sensitivity of the OWT to these foundational effects.

CHAPTER 2

STATIC TWO-DIMENSIONAL ANALYSIS

In this chapter, the development of a static two-dimensional pile foundation model in MATLAB is described and validated by the data obtained from Lesny, Paikowsky, & Gurbuz (2007). The Lesny, Paikowsky, & Gurbuz (2007) model provides the basis for the proceeding analyses in this thesis. The API *p-y* method for sands was used, as it is the most popular design method for pile foundations.

Pile and soil spring geometry were defined by nodal coordinates. From these coodrinates, elements were further defined by cross-sectional area, moment of inertia, and modulus of elasticity. Given boundary conditions and loading, a matrix analysis function from Schafer (2010) formed a linear elastic stiffness matrix and solved

$$\boldsymbol{V_{ff}} = (\boldsymbol{K_{ff}})^{-1}\left(\boldsymbol{F_{ff}} - \boldsymbol{K_{fs}}\boldsymbol{D_s}\right) \tag{2.1}$$

where $\boldsymbol{V_{ff}}$ is the displacement column vector, $\boldsymbol{K_{ff}}$ is the global stiffness matrix, $\boldsymbol{F_{ff}}$ is applied force matrix, $\boldsymbol{D_s}$ is the boundary condition matrix, and the subscript *ff* denotes the unrestrained degrees of freedom.

The soil and pile properties used for analysis can be seen in Table 2.1 and Table 2.2, respectively.

Table 2.1 Properties of Essen Sand (Lesny, Paikowsky, & Gurbuz, 2007)

Symbol	Property	Value
γ'	Submerged Unit Weight	10 kN/m^3
D_R	Relative Density	0.55
k	Initial Modulus of Subgrade Reaction	19,000 kN/m^3
φ'	Friction Angle	40.5°

It should be noted that the value for *k* (see Table 2.1) was estimated using relative density, as opposed to the friction angle (see Figure 1.2). If the friction angle had been used to select *k*, the resulting value would have been approximately 45,000 kN/m^3; consequently, we can state that *k* was picked conservatively.

Table 2.2 Properties of Pile Foundation (Lesny, Paikowsky, & Gurbuz, 2007)

Symbol	Property	Value
b	Pile Diameter	6 m
d	Pile Depth	38.9 m
t	Wall Thickness	0.07 m
a	Cross-Sectional Area	1.304 m^2
I	Moment of Inertia	5.7330 m^4

The force-displacement curves in Figure 2.1 are for a pile represented by four soil springs, where the top curve represents the bottom spring in the model.

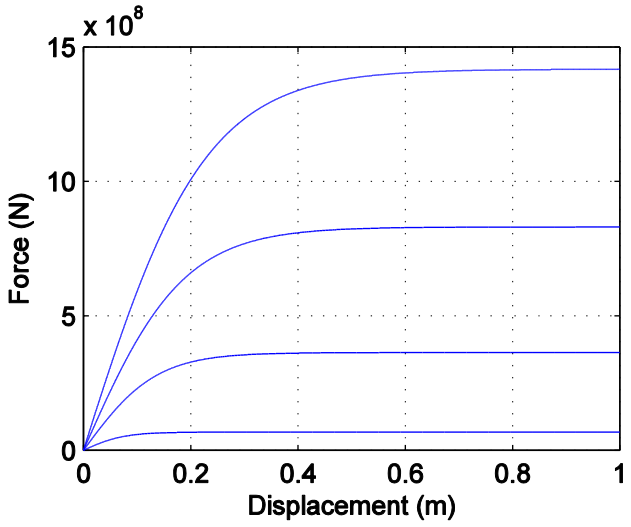

Figure 2.1 Force-displacement Curves for Four-Spring Essen Sand Model

Lesny, Paikowsky & Gurbuz (2007) identified the 50-year loads in Table 2.4 for a 5MW wind turbine situated in the German part of the North Sea. These loads were applied to a pile supported laterally by soil springs and vertically by a roller (preventing downward movement).

Table 2.3. Applied Loads (Lesny, Paikowsky & Gurbuz, 2007)

Symbol	Property	Value
V	Axial Load	35 MN
H	Horizontal Load	16 MN
M	Moment	562 MN-m

To facilitate coding and modeling, the soil springs were assumed to behave linearly, with the stiffness of each spring defined by the initial, linear portion of the force-displacement curve (Section 2.1). Because pile deflections exceeded the linear-elastic range of the force-displacement curves, the linear MATLAB model did not adequately capture soil-pile interaction. Consequently, soil nonlinearity was incorporated into the next model phase using an incremental force-controlled method (Section 2.2). Convergence studies were performed to optimize the model for both accuracy and computational time, with results that agree with the pile head displacement from Lesny, Paikowsky, & Gurbuz (2007) within 4%.

2.1 Static Linear Analysis

The model with applied loads (see Figure 2.2 below) consisted of a four-spring model with soil springs 1 m long connecting the pile to a rigid support. Aside from the convenience of a unit length spring, the spring length was selected to ensure that the serviceability limit state of a horizontal pile head movement of 0.2 m would not be inhibited. A roller support at the bottom of the pile resisted vertical movement of the pile such that the pile alone (and not the bending of the springs) would support the load *V*.

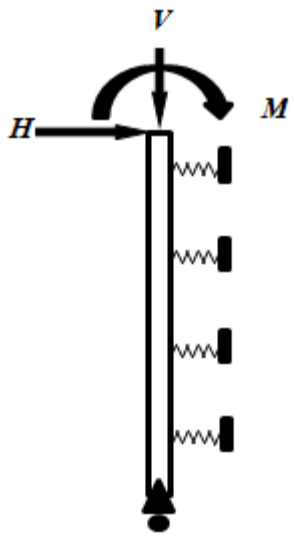

Figure 2.2 Four-Spring Pile Model

Table 2.4 Analysis Results from Linear Four-Spring Model for Pile Head Displacement

Symbol	Property	Value
u	*Horizontal Displacement*	0.0249 m
α	*Rotation*	0.105°

The application of only horizontal load *H* was used to assess whether the assumption of linear soil spring behavior was appropriate, with pile head displacement results listed in Table 2.5.

The top spring node displaced horizontally 0.0231 m. Figure 2.3 displays the force-displacement behavior calculated from the API *p-y* method versus the assumption of linearity.

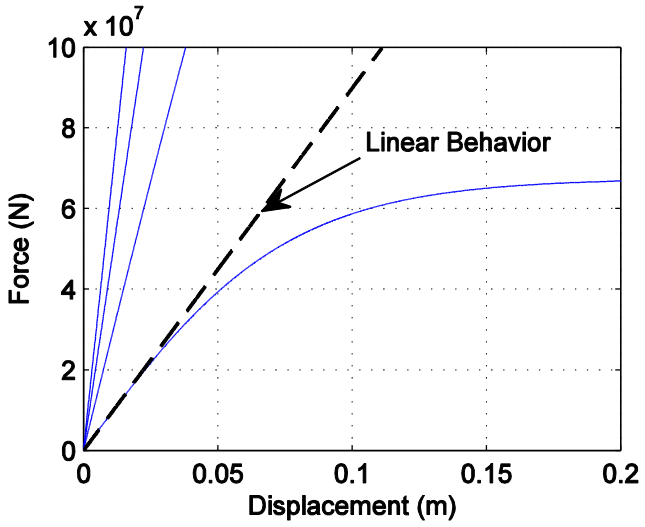

Figure 2.3 Enlarged View of for Four-Spring Essen Sand Model with Linear Behavior

When linear and nonlinear behavior is compared in Figure 2.3, it is inconclusive as to whether or not a linear assumption is appropriate. To quantify the error in the assumption of linear behavior, the nonlinear force-displacement curves were compared to linear spring behavior such that

$$\Delta P = \sum_{i=1}^{n} LR - NLR \tag{2.2}$$

$$LR = x_k kxy \tag{2.3}$$

$$NLR = x_k P(x) \tag{2.4}$$

where *LR* is the linear soil-pile resistance, *NLR* is the nonlinear resistance, x_k is the distance between soil springs, *x* is the depth from the ground surface to the soil spring, *y* is the horizontal displacement at the soil spring, and *P(x)* is the soil-pile resistance per unit length. It should be noted that the absolute value of the horizontal displacement was considered, as soil springs from the opposing face of the pile are assumed to behave identically if the pile were to deflect in the negative-*y* direction.

Using the displacement values from the linear analysis, linear and nonlinear resistances were calculated.

Table 2.5 Results from Linear vs. Nonlinear Comparison

Spring	***y* (x10^{-3} m)**	**LR (x10^{7} N)**	**NLR (x10^{7} N)**	**LR-NLR (x10^{7} N)**
1	14.7	1.32	1.31	0.01
2	3.42	0.924	0.924	0.000
3	0.490	0.220	0.220	0.000
4	0.680	0.428	0.428	0.000
			Sum:	0.01 x 10^{7} N

The summation of the difference between linear and nonlinear resistance for the linear four-spring model is about 1 x 10^5 N (or 100 kN). A convergence study (depicted in Figure 2.4 below) shows that the error converges at 2.1 x 10^6 N with 20 soil springs.

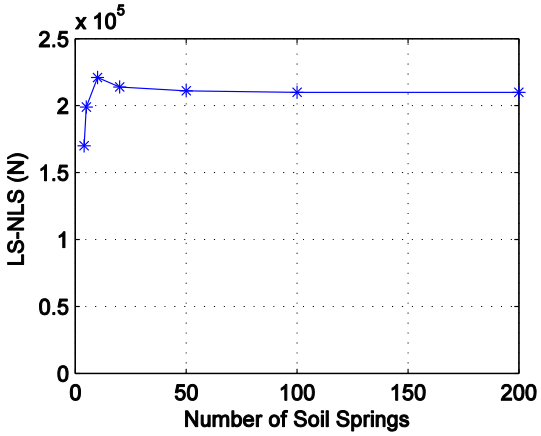

Figure 2.4 Number of Springs vs. Linear-Nonlinear Strength Difference

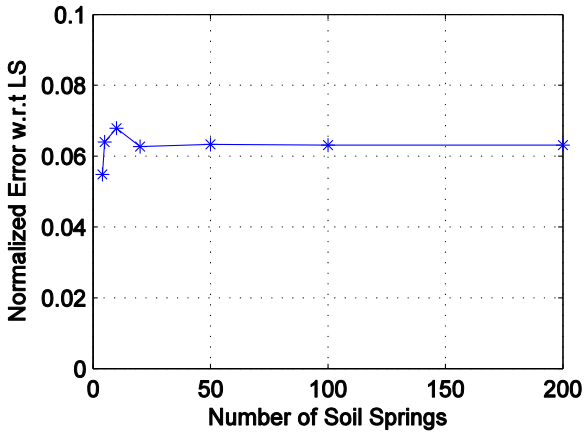

Figure 2.5 Normalized Error vs. Number of Springs

Compared to the horizontal load of 16 MN, the error is equal to 1.3% of the full load and less than 1% of the estimated linear resistance. Using the full loading (with horizontal *H*, vertical *V*, and moment *M* loading), the error in assuming linear behavior increases. When normalized with respect to the linear resistance, the error is approximately 6%. Figure 2.5 shows the convergence of the normalized error with the number of soil springs.

From these convergence studies, we can assume that 20 springs should be sufficiently accurate to model a pile of this length. However, a 20-spring linear analysis with the maximum moment from Lesny, Paikowsky, & Gurbuz (2007) of 855 MN-m applied yielded a horizontal pile head displacement of 0.0983 m, which is nearly 10% stiffer than the published value of 0.109 m (using the *p-y* method). Consequently, assuming linear soil spring behavior is somewhat unconservative, and soil spring nonlinearity must be incorporated into the two-dimensional MATLAB model.

2.2 Static Nonlinear Analysis

Due to the deficiencies of the static linear analysis, a nonlinear analysis was necessary to model soil-structure behavior more accurately. This analysis takes into account the nonlinearity of soil spring behavior, thereby allowing the force-displacement curve of a soil spring to more closely follow the behavior described by the API method.

Soil nonlinearity was introduced by load-controlled sequence. Initially, a single-spring model with a rigid pile was used (see Figure 2.6) with a horizontal load *H* of 2,500 MN applied at the center (at the same depth as the soil spring). This simple model removed the influence of the pile, so *H* could be compared directly to the force-displacement curve from the single soil spring.

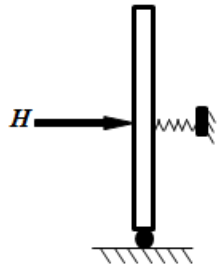

Figure 2.6 Single-Spring Model for Nonlinear Analysis

The total load *H* was divided into even increments, or load steps. The first step was applied and the displacements were processed using the tangential stiffness of the force-displacement curve. This tangential stiffness is taken from the derivative of the *p-y* curve equation with respect to *y* and multiplied by the tributary length of the spring,

$$k_s = x_k \frac{dp}{dy} = x_k \left(-kx \left(\tanh \frac{kxy}{Ap_u} \right)^2 - 1 \right) \tag{2.5}$$

where *y* is the compression of the spring at the instant of load application.

The nodal coordinates of the pile were subsequently adjusted before another load step was applied; displacements and tangential stiffnesses were processed similarly. A 10-step analysis is displayed in Figure 2.7. Note that the nonlinear analysis force-displacement curve stops at the total load *H* of 2,500 MN.

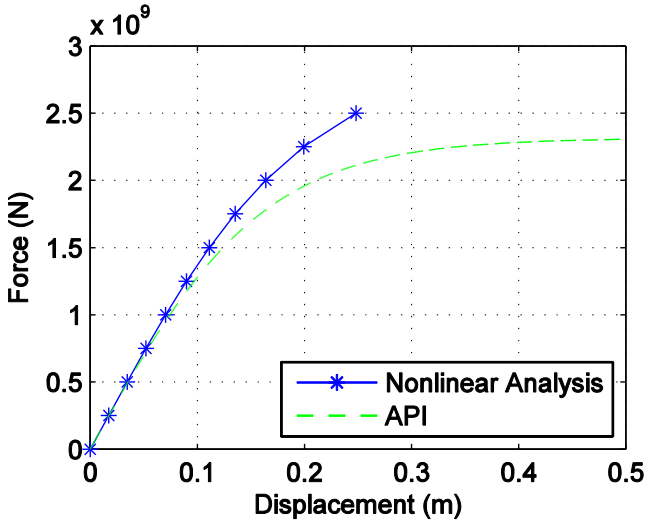

Figure 2.7 Example 10-Step Nonlinear Analysis

The results from the nonlinear analysis show that a given amount of force yields a smaller deflection than the API curve. Due to the fact that each step of the analysis assumes a constant tangential stiffness, it is inevitable that the analysis results from MATLAB will be slightly stiffer than from a strict *p-y* analysis following the API curve (whose tangential stiffness decreases nonlinearly).

A convergence study using the single-spring model was performed with respect to the difference between the API method force-displacement curve and the applied load from the nonlinear analysis, normalized with respect to the applied loading (see Figure 2.8). It was determined that using a 20-step nonlinear analysis would provide sufficient accuracy without sacrificing

computation time. This convergence can also be observed in Figure 2.9, where the full loading was applied to a 20-spring model.

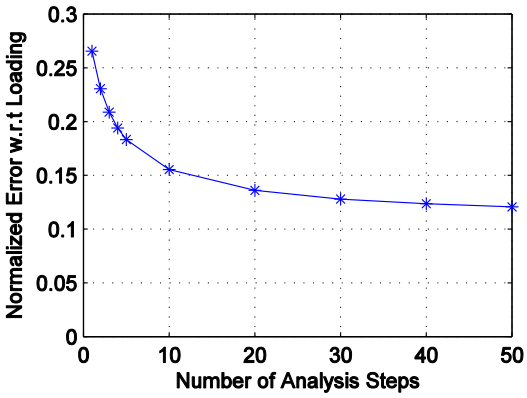

Figure 2.8 Convergence of Nonlinear Analysis for Single-Spring Pile Model

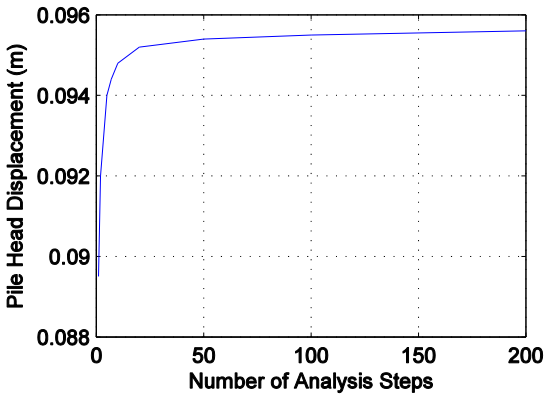

Figure 2.9 Convergence of Nonlinear Analysis for 20-Spring Pile Model

Using 20 soil springs and a 20-step nonlinear analysis, the resulting pile head displacements are as listed in Table 2.7.

Table 2.6 Pile Head Deflections from Nonlinear Analysis

Symbol	Value
u	0.0952 m
α	0.5693°

The results from Table 2.7 were compared and normalized to the force-displacement curves from the API method with a 1.45% error.

2.3 Conclusions

A code was developed in MATLAB to analyze the response of static laterally-loaded OWT pile foundations in sand. Initially, linear soil behavior was assumed using 20 soil springs to represent soil-pile resistance. The resulting pile head displacement was 10% stiffer than the published value

by Lesny, Paikowsky & Gurbuz (2007). To improve accuracy, soil nonlinearity was taken into account by using a force-controlled process. Wind, wave and gravity loads were applied incrementally (as a horizontal force, vertical force, and overturning moment) to the pile head, taking into account the change in soil spring stiffness at each load increment application (step).

Lesny, Paikowsky & Gurbuz (2007) designed a pile for the North Sea loading conditions, whose maximum moment was considered to be 855 MN-m. When this moment was applied to the pile head (neglecting any other loads), the resulting horizontal displacement was 0.109 m. If these same North Sea loading conditions are applied to the MATLAB model (using 20 springs and a 20-step load application analysis), the pile head displaces 0.1044 m. Given a discrepancy of approximately 4% (as compared the 10% error from the linear analysis), we can appropriately consider this MATLAB model to be calibrated.

It should be noted that the digitization of the API figures (which was necessary in order to automate the creation of *p-y* curves) lead to a higher estimation for *k* as a function of relative density (20,800 kN/m^3, as opposed to 19,000 kN/m^3). For this value of *k*, the static nonlinear horizontal displacement is 0.1014 m, which is 7% stiffer than the Lesny, Paikowsky, & Gurbuz result. This difference is considered acceptable for continued use of automated *p-y* curves.

CHAPTER 3

PILE FOUNDATION RELIABILITY

The reliability index (β) is often used to more concisely express small probabilities of failure. The probability of failure can be calculated from β by

$$p_f = \Phi(-\beta) \tag{3.1}$$

where p_f is the probability of failure and Φ is the normal cumulative distribution function. Using a first order reliability method, β can be estimated from the mean and standard deviation of the safety margin, which is a function of limit state. For OWTs, these limit states are divided into two main categories: ultimate limit states and serviceability limit states.

Typically, β for OWTs is 4, which corresponds to p_f = 3.1671 x 10^{-5} or approximately 1 in 31,574 (Stuyts, Vissers, Cathie, & Jaeck, 2011). Phoon (2008) explains that this value of β corresponds to a 50-year OWT design life and an ultimate limit state. For serviceability limit states, the target β is 1.5 (p_f = 0.1587), corresponding to a 1-year return period (Phoon, 2008).

Ultimate limit states describe a condition which results in the destructive failure of an OWT, whereas serviceability limit states merely indicate that the OWT will be unable to function efficiently and effectively under those conditions. The serviceability limit states commonly used for OWT pile foundations restrict pile head displacement (u) to 0.2 m horizontally or 0.7° of rotation (α). Using these criteria for failure, they can be written in terms of the safety margins

$$g_1(u) = 0.2 - u \tag{3.2}$$

$$g_2(\alpha) = 0.7 - \alpha \tag{3.3}$$

These safety margins are a function of loading, pile bending stiffness, and soil-pile resistance. In reliability based design of OWTs, both loading and soil are can be considered random.

Using beta distributions to characterize variability in friction angle (φ') and a Weibull distribution for load variability, sensitivity analyses are performed using the two-dimensional model validated in Chapter 2.

3.1 Soil Variability

Soil variability is spatial, not random. Characterizing spatial soil variability with random processes transfers soil property uncertainty from epistemic to aleatory, facilitating modeling and greatly assisting engineers in their ability to use geotechnical data for design.

The normal, or Gaussian, probability distribution is commonly used to model variability in soil properties, partially because it simplifies calculations. However, non-Gaussian distributions are useful as many soil properties are bounded by particular ranges (e.g., non-negative values) or are skewed. Beta, gamma, and lognormal distributions are often used.

Due to the variability of soil properties from site to site (and within a site), Baecher & Christian (2003) caution that it is neither "easy nor wise to apply typical values of soil property variability… for a reliability analysis." The study of pile foundation reliability that proceeds in this thesis is based upon minimal data, which would be insufficient for design. For a realistic pile design, site-specific geotechnical data is a necessity. Trends would then be fit to the data, likely characterized using an autocovariance or autocorrelation function. Pile design would proceed based upon the findings from this type of data analysis.

Without a detailed site investigated from the North Sea site selected by Lesny, Paikowsky & Gurbuz (2007), the following reliability analyses are more academic than they are realistic. However, despite the lack of geotechnical data, sensitivity analyses can be conducted to monitor the response of β with respect to soil property distribution, pile parameters, and loading.

Soil properties are assumed to be horizontally homogeneous but vertically heterogeneous.

3.1.2. **Variation in Friction Angle**

Introducing randomness in φ' produces a significant effect on API *p*-y curves, and consequently soil-pile resistance, of a monopile foundation.

Phoon (2008) and Baecher & Christian (2003) proposed coefficient of variation (COV) ranges for φ' as listed in Table 3.1, with

$$COV = \frac{\mu}{\sigma} \tag{3.4}$$

where σ is the standard deviation and μ is the mean.

Table 3.1 COV Ranges for Friction Angle (Phoon, 2008)

Property Variability	COV (%)
Low	5-10
Medium	10-15
High	15-20

Lacasse & Nadim (1996) report the COV range in effective φ' for sands (based on laboratory tests) to be between 2-5% and Sett & Jeremić (2009) state that 30% is commonly observed. The variation in COV is in part due to the method of measuring φ', but also because some of these ranges consider both sands and clays. Because the following analysis focuses on soil-structure interaction in sands, the 5% COV listed by Lacasse & Nadim for sands will be the maximum considered COV.

3.1.3. **Variation in Relative Density**

The relative density of a soil is computed by

$$D_R = \frac{e_{max} - e}{e_{max} - e_{min}} \quad \textbf{(3.5)}$$

where e_{max} is the maximum void ratio for a given soil, e_{min} is the minimum void ratio for the soil, and e is the *in situ* void ratio, as measured using a standard laboratory test procedure (e.g., ASTM D4253 and D4254). Levels of soil density are classified per Table 3.2.

Table 3.2 Density Classification of Soil (Liu & Evett, 2004)

Relative Density	Density Classification
<15%	Very Loose
15-35%	Loose
35-65%	Medium Dense
65-85%	Dense
85%<	Very Dense

Uzielli (2007) reports that the mean relative density (D_R) for sand is typically between 30-70% with a COV ranging from 10-40%.

A proposed relationship between φ' and D_R is listed below (Equation 3.6) for D_R more than 35% (Rankine, Sivakugan, & Cowling, 2006).

$$\varphi' = 19D_R^2 + 33 \quad \textbf{(3.6)}$$

This relationship was proposed for hydraulic mines in Australia with consistent properties. Skempton (1986) and Meyerhof (1957) also proposed relationships between the square of D_R and

φ', but these equations produce significantly lower values for φ' (by approximately a factor of 2). Taken out of context, using any of these relationships is probably not appropriate.

API implies a relationship between φ' and D_R as seen in Figure 3.1.

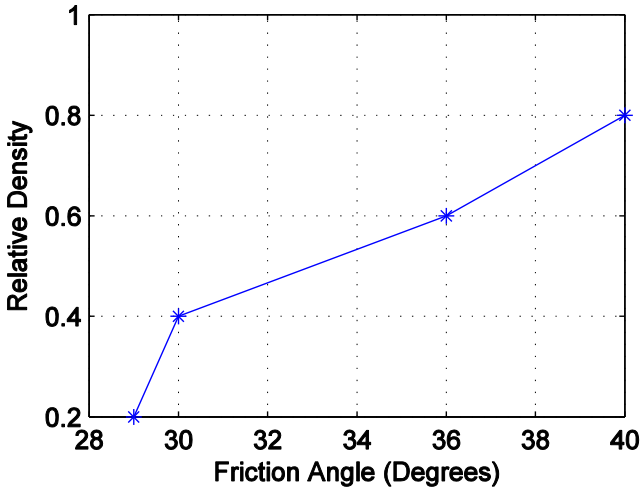

Figure 3.1 Relative Density vs. Friction Angle

This relationship is displayed as piecewise linear, matching the values given for φ' at the top of Figure 1.2 with the values at the bottom for D_R.

It is evident that the relationship between loose sand (with φ' less than 30°) is different from medium dense to dense sands (with a range of φ' from 30° to 40°). The Essen Sand analyzed in Chapter 2 (see Table 2.3) displays characteristics of both medium dense and dense sand: If characterized by relative density, Essen Sand is medium dense; however, if characterized by φ' (see Figure 1.2), API would consider Essen Sand to be dense. Categorically, a sand which is classified as either medium dense or dense will not behave as a loose sand.

Because the vast majority of OWT foundation research considers sites with medium dense to dense sands, the range of φ' and D_R characterizing loose sand will be neglected.

A best-fit curve for the relationship between φ' and D_R for medium dense to dense sands (illustrated in Figure 3.1) was numerically approximated in Excel by the equation

$$\varphi' = 20.2{D_R}^2 + 27.9 \tag{3.7}$$

which mimics Equation 3.6, with a similar coefficient for the D_R^2 term.

In reality, relative density drives φ'; however, establishing D_R as a deterministic variable (D_R as a function of φ') allows us to consider φ' as the sole random soil property. For the proceeding analyses, Equation 3.8 uses three terms to describe the relationship between φ' and D_R, capturing the relationship more closely

$$D_R = 0.0014\varphi'^2 - 0.0594\varphi' + 0.9176 \tag{3.8}$$

3.1.4. **Effect of Friction Angle on Pile Head Reaction**

To consider the basic relationships between φ' and both pile head displacement and rotation for medium-dense to dense sands, φ' was considered to be perfectly correlated for Figures 3.2 and 3.3.

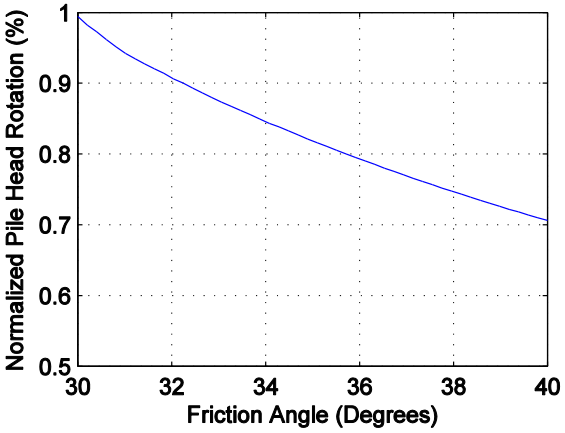

Figure 3.2 Normalized Pile Head Rotation as a

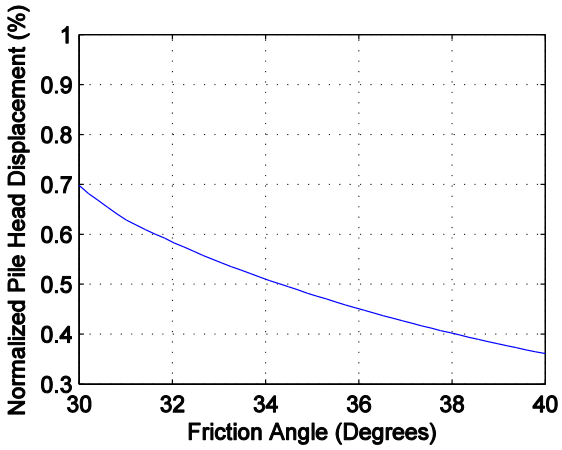

Figure 3.3 Normalized Pile Head Displacement as a

Function of Friction Angle **Function of Friction Angle**

Both figures were normalized with respect to the serviceability limits of 0.7° of rotation and 0.2 m of horizontal displacement.

Note that in Figure 3.2, the maximum rotation (at φ' = 30°) is just less than the serviceability limit; in Figure 3.3, the maximum displacement reaches only 70% of the limit. We can expect that rotation is likely to control reliability given the range of medium-dense to dense sands (φ' = 30°-40°) since the serviceability limit consideration rotation is far closer to being exceeded than the serviceability limit for horizontal displacement.

3.2 Static Reliability Analysis

This section utilizes the static nonlinear model from Chapter 2, which was adapted to analyze the reliability of an OWT pile foundation. The applied pile design and loads were those calculated by Lesny, Paikowsky & Gurbuz (2007).

Beta distributions were used to characterize the random generation of φ', with a lower bound of 30° and upper bound of 40° (representing the range for medium dense to dense sands). The beta distribution probability density function (PDF) is characterized by Equation 3.9,

$$f(\varphi'|A,B) = \frac{1}{Beta(A,B)}\varphi'^{A-1}(\varphi'-1)^{B-1} \quad \textbf{(3.9)}$$

where A and B are distribution parameters. By using different values of A and B, an infinite number of distribution shapes can be achieved.

The second moment properties of the safety margins g_1 and g_2 (Equations 3.2 and 3.3) were estimated via Monte Carlo (MC) simulation. The reliability indices (β_1 and β_2) were then

calculated by dividing the mean of the safety margin (μ_g) by the standard deviation (σ_g) of the safety margin (See Equations 3.10 and 3.11 below).

$$\beta_1 = \frac{\mu_{g1}}{\sigma_{g1}} \tag{3.10}$$

$$\beta_2 = \frac{\mu_{g2}}{\sigma_{g2}} \tag{3.11}$$

3.2.1 **Correlated Friction Angle Variation**

Correlation in soil properties is somewhat dependent on soil type and testing method, and extremely site-dependent (Uzielli, Lacasse, Nadim, & Phoon, 2007).

Without a site investigation, we are unable to model a realistic site; however, we can statistically model variation of φ' with a stationary, non-Gaussian translation process model

$$\varphi'(x) \sim \left(F_{\varphi'}(\varphi'), C_{\varphi'\varphi'}(|x_1 - x_2|)\right) \tag{3.12}$$

Where $F_{\varphi'}$ is the cumulative distribution function representing φ', $C_{\varphi'\varphi'}$ is the covariance matrix and x_1 and x_2 are two points along the length of the pile.

Without knowing exactly how φ' varies vertically along the length of the pile, two limiting cases were considered: perfect correlation and independent variation (white noise process). In terms of Equation 3.13, independent variation is when $C_{\varphi'\varphi'}$ is zero, and the opposing assumption of perfect correlation is when $C_{\varphi'\varphi'}$ is one.

A convergence study was performed to determine the minimum number of samples suitable for estimating β, considering a site with mean φ' of 35° and COV of 5% (see Figure 3.4). In the case of perfectly correlated soil conditions, a random value of φ' was generated (as characterized by the PDF in Figure 3.4) per sample and remains constant for the full length of the pile, making φ'

constant for all soil springs. For independent variation, the variation of φ' along the length of the pile is described by a white noise process with randomly generated values of φ' (with distribution described by Figure 3.4) for each soil spring.

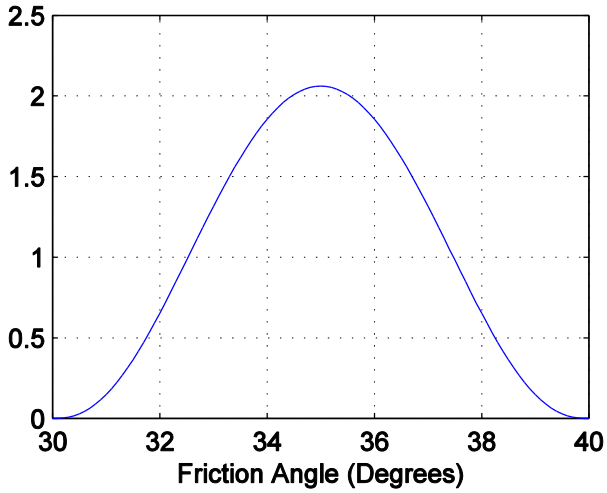

Figure 3.4 Beta Probability Density Function, 5% COV

Different estimates of β were produced based on a certain number of samples. The rotation reliability index (β_2) controlled per expectation (given Figure 3.2 and 3.3), with β_1 larger than β_2 by a factor of three or more. While the total probability theorem would require us to take into account both reliability indices, β_1 will be considered negligible and reliability will be assessed per Equation 3.9.

$$\beta \approx \beta_2 \tag{3.13}$$

In order to determine the number of samples necessary to estimate β, the standard deviation of twenty estimations of β was calculated for several sample sizes.

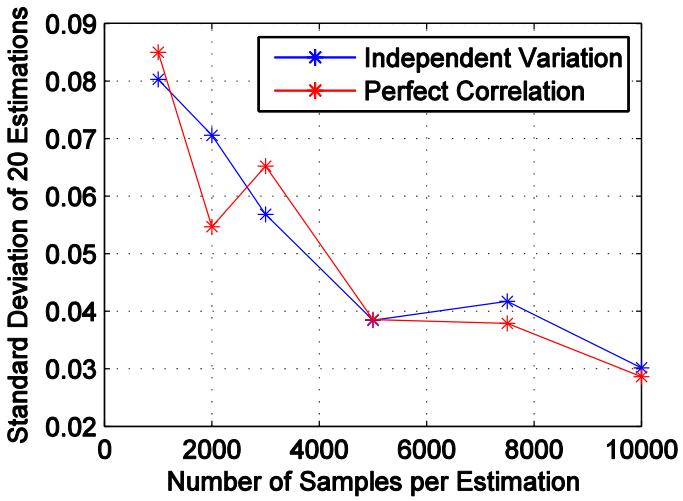

Figure 3.5 Standard Deviation of Reliability Index vs. Number of Samples Considering Friction Angle Variation

The cases of perfect correlation and independent variation demonstrate very similar behavior in the convergence studies depicted in Figure 3.5. While both curves show convergence at approximately 5,000 samples, 10,000 samples are required to produce a consistent estimation of β within a tolerance of 0.1.

Proceeding analyses will use 10,000 samples to estimate β.

The resulting reliability indices of these two cases are shown in Table 3.3.

Table 3.3 Comparison of Results from Correlation Limiting Cases

$C_{\varphi\varphi}$	μ_α	σ_α	β	p_f
0	0.576	0.027	4.6	1.0141×10^{-5}
1	0.575	0.033	3.8	2.9195×10^{-4}

It is evident from the discrepancy between the two values of β (and consequently probability of failure, p_f) that correlation plays a significant role in the reliability analysis. While both analyses yielded approximately the same mean pile head rotation, the standard deviation of the response was higher for the perfectly correlated case. The histograms below (Figures 3.6 and 3.7) illustrate

the wider spread of rotations experienced by the pile head when φ' variation is modeled with perfect correlation.

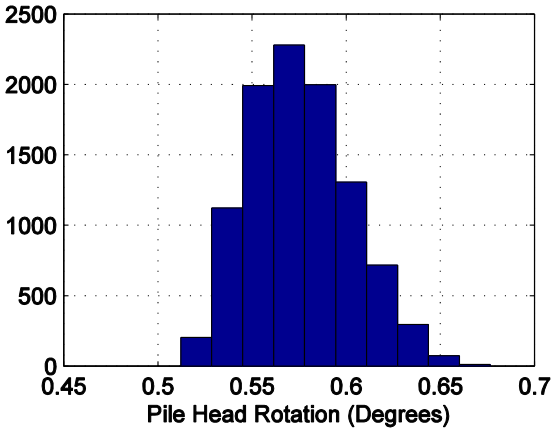

Figure 3.6 Histogram of Independent Variation Pile Head Rotation

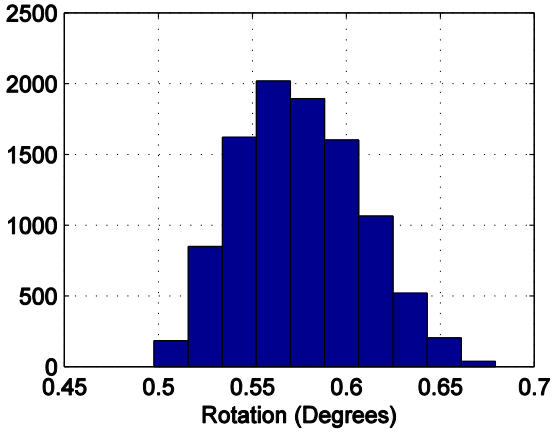

Figure 3.7 Histogram of Perfect Correlation Pile Head Rotation

Consider pile head rotation as a function of φ' (refer to Figure 3.2): because $\mu_{\varphi'}$ for all independent variation samples is approximately 35°, the range of pile head rotations in Figure 3.6 is understandably narrower than the range of perfectly correlated samples in Figure 3.7 where $\mu_{\varphi'}$ is less than 35° for approximately 50% of the samples.

Correlation should not be ignored in reliability analyses, as evidenced by the results above. Proceeding analyses in this thesis will present the limiting cases to gauge the potential range of β, but the primary assumption will be perfect correlation of φ' along the length of pile.

3.2.2 **Effect of Friction Angle Variance**

The effect of φ' variance on reliability was examined, considering the medium dense to dense sand range (30°-40°) and a mean φ' ($\mu_{\varphi'}$) of 35°. Figure 3.8 demonstrates the beta PDFs with COV values ranging from 2-8% and then 8.25% (see Table 3.4 for distribution parameters). This

range was selected based on the minimum COV of 2% from Lacasse & Nadim (1996) and the maximum COV 8.25% representing a uniform distribution.

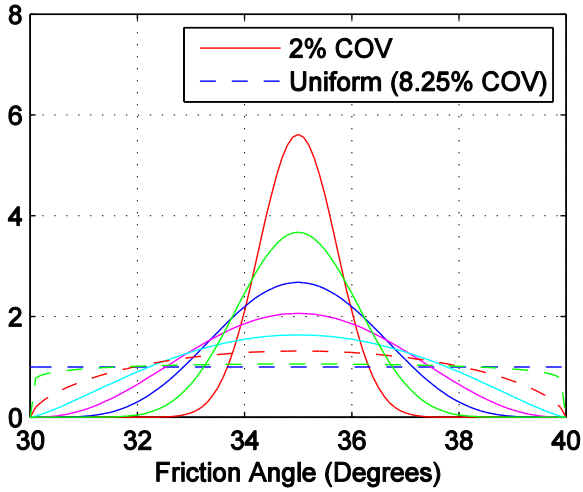

Figure 3.8 Beta Probability Density Functions Representing COVs 2-8.25%

Table 3.4 Beta Distribution Parameters to Examine Effect of Variance

μ (°)	σ (°)	COV (%)	*A*	*B*
35	0.7	2	25	25
35	1.05	3	10.834	10.834
35	1.4	4	5.875	5.875
35	1.75	5	3.577	3.577
35	2.1	6	2.334	2.334
35	2.45	7	1.587	1.587
35	2.8	8	1.095	1.095
35	2.8875	8.25	1	1

Considering all of these symmetrical distributions (as well as the uniform distribution), an analysis using 10,000 samples was completed for both the independently varying and perfectly

correlated φ' cases (see Figure 3.9). As the COV of the beta distribution for φ' increases, β decreases nonlinearly.

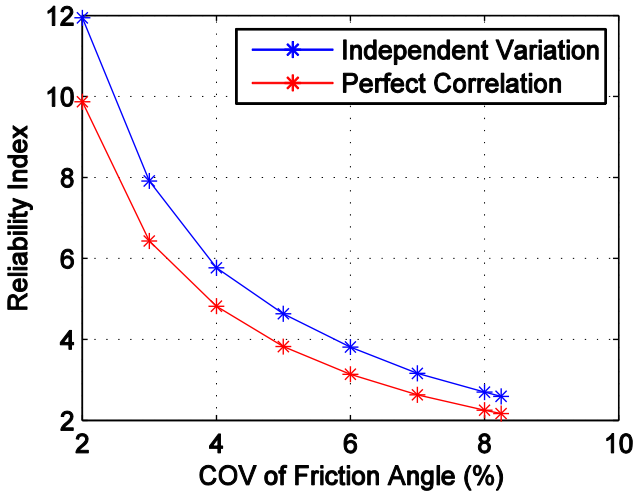

Figure 3.9 Reliability Index vs. COV of Friction Angle

If we consider the target β to be 4 (in accordance with the 50-year return period used for the loading), the pile design from Lesny, Paikowsky & Gurbuz (2007) would be considered appropriate for symmetrically beta distributed soil conditions with $\mu_{\varphi'}$ = 35° and COV between 5 and 6% (bounded by the limiting cases).

The nonlinearity of the reliability problem is emphasized in Figure 3.10, where mean pile head rotation from 10,000 samples is compared to the COV of the φ' distribution. While the difference between minimum and maximum rotations in this range is less than 0.01° (approximately 1.2% of the maximum rotation), $\mu_{\varphi'}$ is constant at 35°. The output of pile head rotation increases with variation, despite constant mean input.

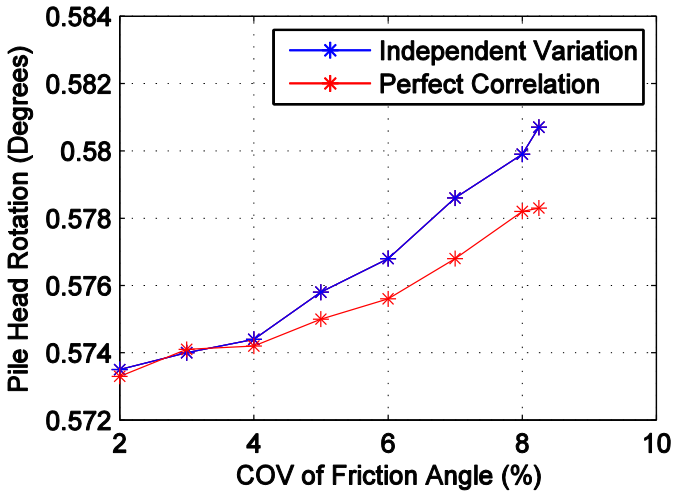

Figure 3.10 Mean Pile Head Rotation vs. COV of Friction Angle Distribution

3.2.3 **Effect of Friction Angle Distribution Shape**

One of the main benefits of a beta distribution is in its flexibility, both in distribution shape and because it can be bounded above and below. We have focused on a particular range of φ' values (30°-40°), but there are an infinite number of possibilities for the shape of the beta PDF representing φ'. The previous section examined the effect of variance on reliability, considering the mean to be centered at 35°; changing the shape of the PDF will change both the mean and variance of φ'. The range of beta distribution parameters A and B considered (see Table 3.5) range from 1 to 3.577, as $A = B = 3.577$ is equivalent to a symmetrical 5% COV beta distribution. The type of case examined in Section 3.2.2 can be seen on the diagonal, where the parameters A and B are of equal value ($\mu_{\varphi'} = 35°$). The values used for A and B were even spaced along the interval 1 to 3.577.

Table 3.5 Mean and Standard Deviation of Friction Angle with Respect to Beta Parameters

		B					
	μ, σ	1	1.5154	2.0308	2.5462	3.0616	3.5770
A	1	35.00, 2.89	33.98, 2.61	33.30, 2.34	32.82, 2.11	32.46, 1.91	32.18, 1.75
	1.5154	36.03, 2.61	35.00, 2.49	34.28, 2.32	33.73, 2.15	33.31, 1.99	32.98, 1.85
	2.0308	36.70, 2.34	35.73, 2.32	35.00, 2.22	34.44, 2.10	33.99, 1.98	33.62, 1.87
	2.5462	37.18, 2.11	36.27, 2.15	35.56, 2.10	35.00, 2.03	34.54, 1.94	34.16, 1.85
	3.0616	37.54, 1.91	36.69, 1.99	36.01, 1.99	35.46, 1.94	35.00, 1.87	34.61, 1.81
	3.5770	37.82, 1.75	37.03, 1.85	36.38, 1.87	35.84, 1.85	35.38, 1.80	35.00, 1.75

Reliability surfaces for the independent variation and perfect correlation cases can be seen in Figures 3.11 and 3.12, illustrating the increase in β as A increases and B decreases.

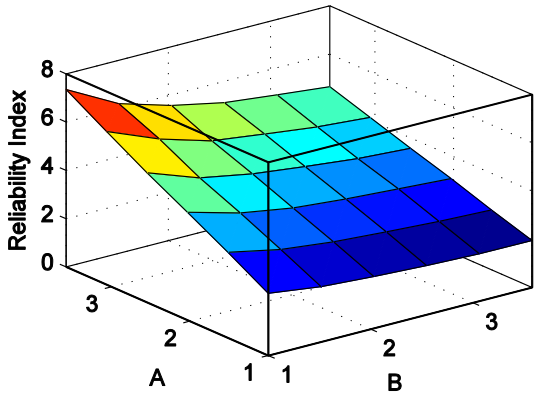

Figure 3.11 Reliability Surface Considering Beta Parameters, Independent Variation Case

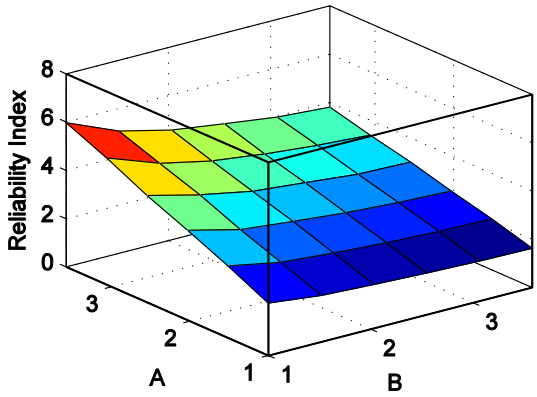

Figure 3.12 Reliability Surface Considering Beta Parameters, Perfect Correlation Case

The general shape and behavior of both surfaces is similar, excepting the fact that the independent variation case rises more steeply into the higher values of β than the perfect correlation case. There is little difference between β values when A is 1, but independent variation causes β to rise to higher values than the perfect correlation case when A is 3.577.

Contours in Figures 3.13 and 3.14 confirm that as *A* increases (given a constant value of *B*), β increases more rapidly for the independently varying case than perfectly correlated case.

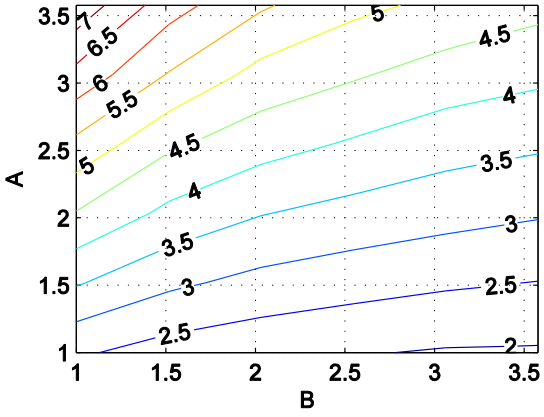

Figure 3.13 Contour Plot of Reliability Indices with Respect to Beta Parameters , Independent Variation Case

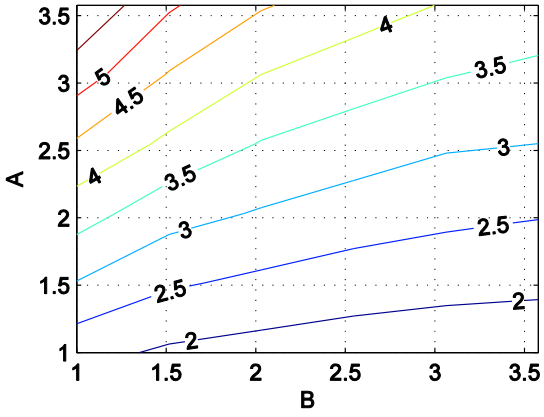

Figure 3.14 Contour Plot of Reliability Indices with Respect to Beta Parameters, Perfect Correlation Case

At its most dramatic, β rises from approximately 2.5 to 7 (seen in Figure 3.13 when *B* is 1). As *B* increases with constant *A*, β decreases slightly; even at the maximum considered value of *A* (3.577), this change is from 7 to approximately 4.5.

We can conclude that reliability is more sensitive to variation in the *A* parameter of the beta distribution than the *B* parameter, regardless of correlation case. Knowing that increasing the COV of φ' causes a nonlinear decrease in β (refer to Figure 3.7), the maximum COV of 5% (per Lacasse & Nadim, 1996) will yield the most conservative value for β. A contour plot of φ' COV considering various combinations of *A* and *B* is illustrated in Figure 3.15.

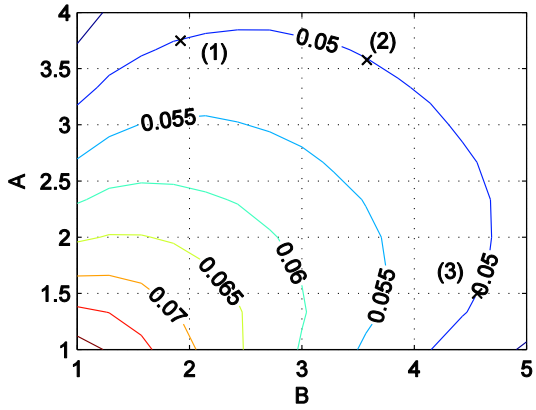

Figure 3.15 Contours of Friction Angle COV with Respect to Beta Parameters

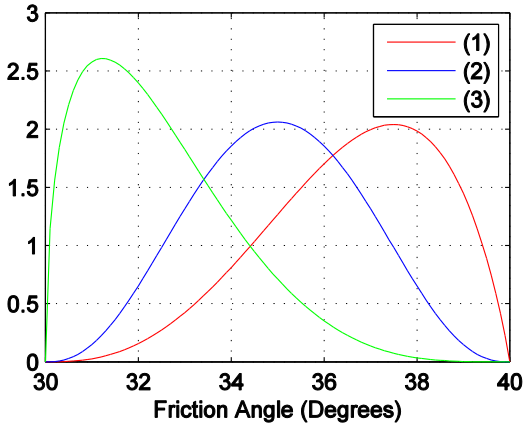

Figure 3.16 Beta Probability Density Functions with Approximately 5% COV per Table 3.5

Three points along the 0.05 (5%) contour have been selected to demonstrate how distribution behavior changes with the selection of *A* and *B* (see Table 3.6 and Figure 3.16). As *A* increases, the mean of the distribution shifts right, as evidenced in Figure 3.16.

Table 3.6 Beta Parameters Yielding Approximately 5% COV

Point	A	B	β Independent Variation	β Perfect Correlation
1	3.75	1.92	5.9	4.8
2	3.577	3.577	4.6	3.8
3	1.5	4.56	2.4	2.0

Analyzing several points along 5% contour line from Figure 3.15, it is evident that as $\mu_{\varphi'}$ increases, β increases linearly for both cases (see Figure 3.17).

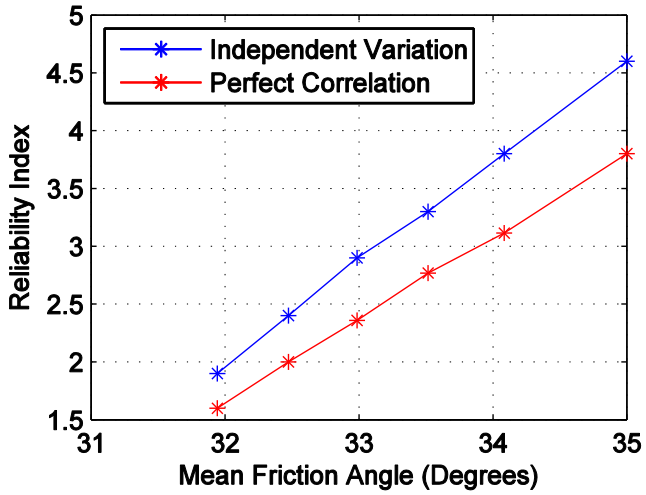

Figure 3.17 Reliability Index vs. Mean Friction Angle

The most conservative distribution of φ' to assume would be the 5% COV distribution with the lowest mean value; however, without detailed information from a designated soil site, this choice is somewhat arbitrary. Given this context, proceeding analyses will assume the simple symmetric 5% COV distribution with $\mu_{\varphi'}$ = 35°. This distribution yields a range of β from 3.8 to 4.6 (depending on vertical spatial correlation), considering a loading return period of 50 years and pile head serviceability limits.

3.2.4 **Effect of Pile Parameters**

Section 3.2 focused primarily on the effects of soil properties and variation on reliability. In realistic design scenarios however, pile properties are selected based on the results of a site investigation. This section focuses on the effect of pile property selection on reliability, considering pile diameter, wall thickness, and embedment depth. The soil (as previously discussed in Section 3.2) is characterized by a beta distribution with $\mu_{\varphi'}$ of 35° and 5% COV, ranging from 30°-40° (see Figure 3.4).

A range of diameters from 6 m to 7 m and wall thicknesses from 0.06 m to 0.08 m were analyzed and are represented by the reliability surfaces in Figures 3.18 and 3.19 (considering the limiting cases of independent variation and perfect correlation, respectively).

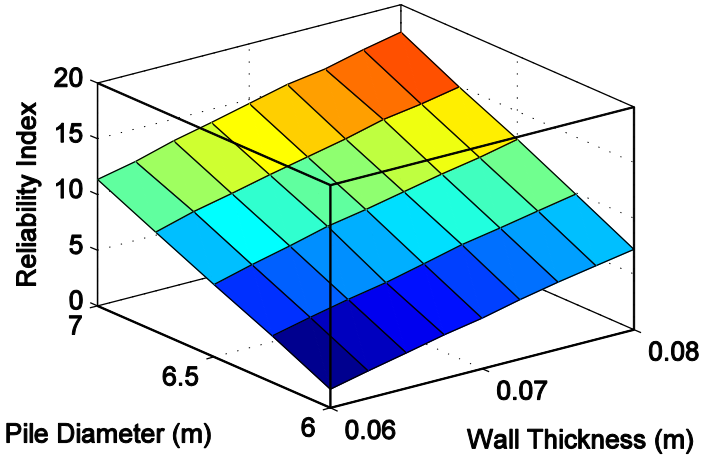

Figure 3.18 Reliability Surface Considering Pile Diameter and Wall Thickness, Independent Variation Case

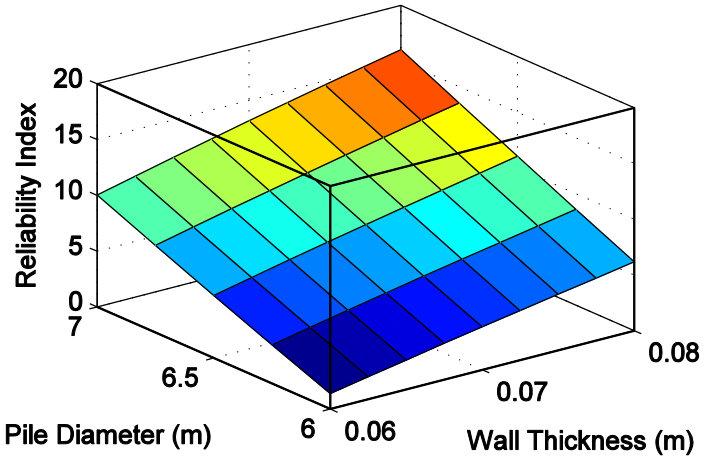

Figure 3.19 Reliability Surface Considering Pile Diameter and Wall Thickness, Perfect Correlation Case

Predictably, increasing pile diameter and wall thickness raises β for both cases. The maximum and minimum β values from the independent variation and perfect correlation cases are listed below in Table 3.7.

Table 3.7 Maximum and Minimum Reliability Indices Considering Pile Diameter and Wall Thickness

Case	β_{max}	β_{min}
Independent Variation	17.6	1.7
Perfect Correlation	16.0	1.4

As pile diameter and wall thickness dictate the moment of inertia (and therefore the bending capacity) of the pile, contour plots were made of the surfaces in Figures 3.18 and 3.19 to examine the sensitivity of β to bending capacity (see Figures 3.20 and 3.21).

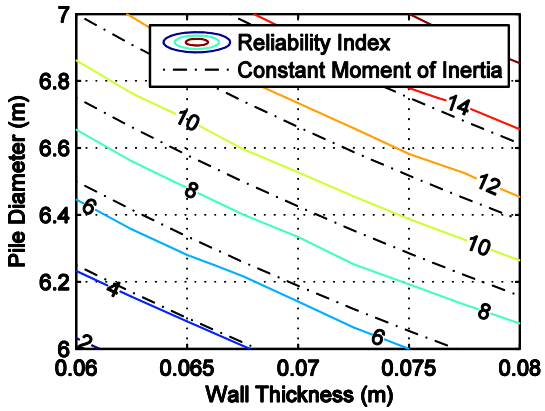

Figure 3.20 Contours of Reliability and Moment of Inertia, Independent Variation Case

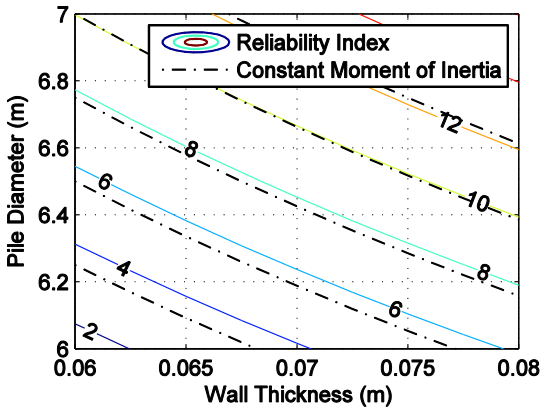

Figure 3.21 Contours of Reliability and Moment of Inertia, Perfect Correlation Case

The near-parallel reliability and moment of inertia contours of Figures 3.20 and 3.21 indicate that while soil-pile resistance is a function of pile diameter, the contribution of a pile's moment of inertia is the more substantial influence on β. If the pile diameter effect on soil-pile resistance were more influential, non-parallel behavior would be exhibited in the contour relationship of reliability and moment of inertia.

The effect of embedment depth on reliability was also analyzed, using the pile cross-section properties from Lesny, Paikowsky, & Gurbuz (2007). The distance between soil springs (x_k) was held approximately constant for the range of embedment depths considered (30-45 m), dividing the analyzed depth by the x_k determined from the convergence studies for the 38.9 m Lesny, Paikowsky & Gurbuz pile (1.945 m) and rounding to the nearest whole number of soil springs. Figure 3.22 illustrates that as embedment depth increases, β converges for both cases around 36 m of embedment.

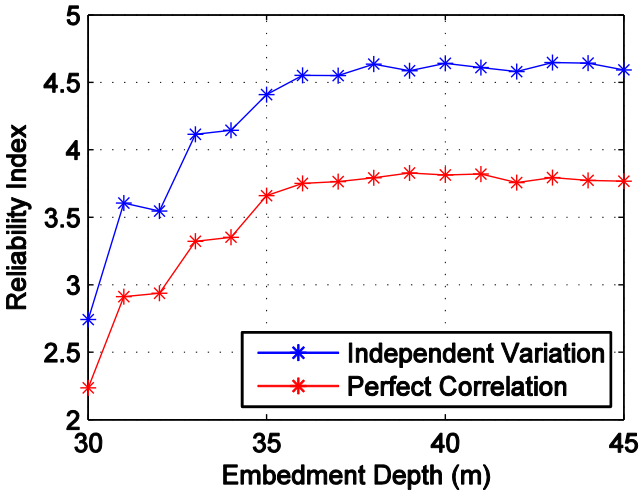

Figure 3.22 Reliability Index vs. Embedment Depth

These results support the previous analysis which considered the Lesny, Paikowsky & Gurbuz (2007) pile with 38.9 m of embedment.

3.2.5 **Load Variation**

Similar to cases of soil variation, the absence of site-specific wind and wave data means that the following sensitivity analysis should be considered academically. The applied horizontal load and overturning moment would be calculated from site-specific wind and wave distributions, allowing for a more realistic overview of how load varies.

Without this information, a topical study of load variation was conducted assuming constant load values per Lesny, Paikowsky & Gurbuz (2007) and a constant φ' of 35° for the full length of the pile. Table 3.8 compares the influence of the horizontal load H to the overturning moment M acting at the mudline, with vertical load V applied in both cases. Given the long moment arm that the tower creates when compared to the fixity at the mudline, the overturning moment is the most influential factor.

Table 3.8 Loading Influence on Pile Head Response

Pile Head Response	Response from H	Response from M	Full Response
u	0.0238 m	0.0659 m	0.0958 m
% of Full Response	24.8%	68.8%	100%
α	0.1026°	0.4488°	0.5730°
% of Full Response	17.9%	78.3%	100%

The loads given by Lesny, Paikowsky, & Gurbuz (2007) are calculated from 50-year return periods of wind and wave loading. It is not economical to design for the highest loads that OWTs may experience, and as such probability and return periods are used to mitigate the risk of under-designing while managing the possibility of wasting resources in overdesign.

To consider the sensitivity of an OWT pile foundation to loading, the 50-year return period load values calculated by Lesny, Paikowsky, & Gurbuz (2007) were treated as mean values with variation about the mean described by a Weibull distribution. Weibull distributions are commonly used to model PDFs for long term wind data. Because the vertical loading on an OWT pile foundation is due to gravity loading, it can be considered deterministic. The mudline loads H and M are attributed to wind and waves, making them probabilistic loads.

Assuming a 5% COV and perfect correlation between the two probabilistic loads (*H* and *M*), a convergence study was performed to determine the appropriate number of samples necessary to determine β. In Figure 3.23, soil properties were assumed to be constant (φ' = 35°).

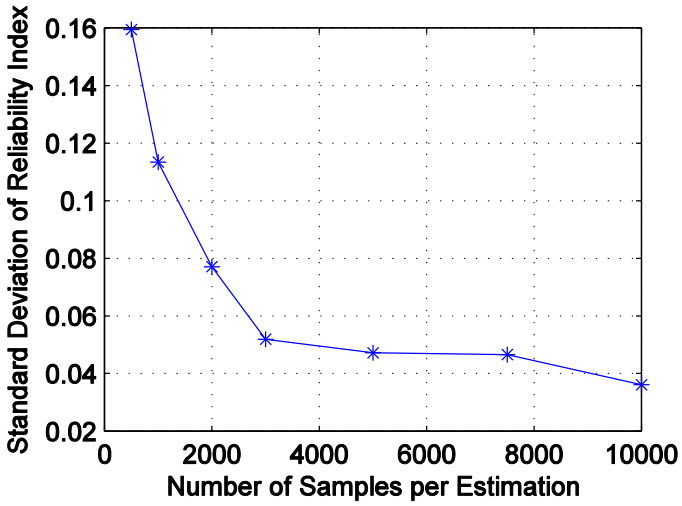

Figure 3.23 Standard Deviation of Reliability Index vs. Number of Samples Considering Load Variation

Similar to the convergence study regarding the number of samples required to model soil variation, Figure 3.23 indicates that 10,000 samples are necessary to achieve convergence in the standard deviation of β, considering the results of 20 estimates. Considering perfectly correlated soil properties (φ' = 35°) and 5% COV loading, $\beta = 4.1$.

The 5% load COV was selected such that the influence of loading and φ' could be compared. When depicted next to the convergence studies for φ', Figure 3.24 demonstrates that the standard deviation of β considering load variation is similar to the studies considering variation in only φ'.

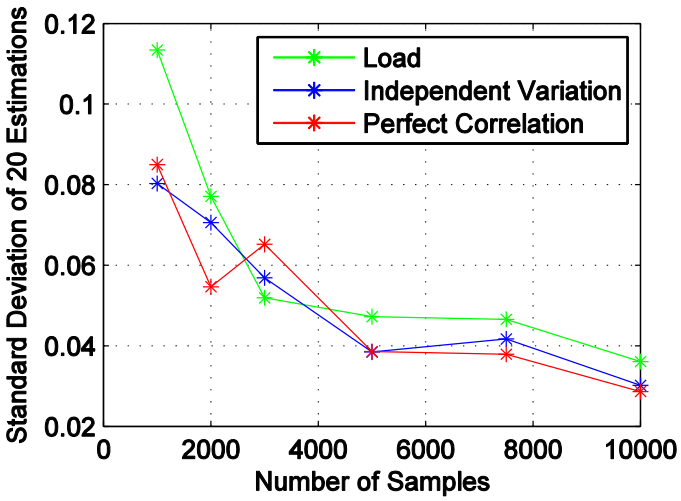

Figure 3.24 Comparison of Load and Friction Angle Convergence Figures

As discussed previously however, realistic design situations involve randomness in both the soil and loading conditions. A convergence study comparison including all of these factors can be seen below in Figure 3.25.

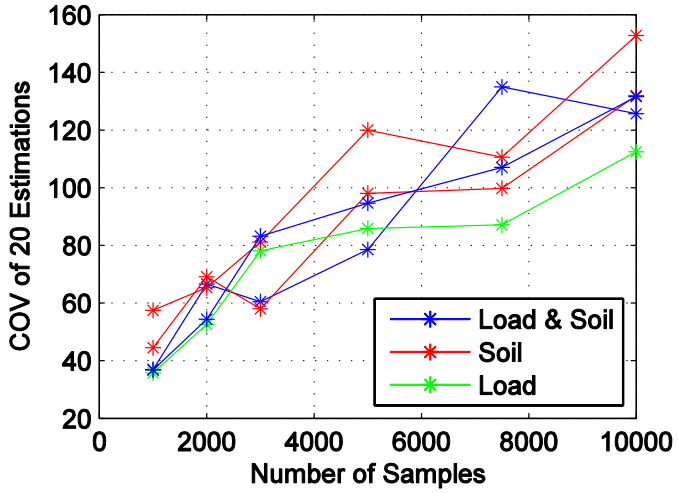

Figure 3.25 Comparison of Convergence Studies Considering Combinations of Load and Soil Randomness

Differentiation between the independent variation and perfect correlation soil convergence studies were neglected as they have displayed consistent convergence behavior with one another for every case.

The trend of Figure 3.25 illustrates that the COV of β converges in a similar manner despite the varying sources of randomness. While larger numbers of samples (or an increased number of estimations) would reduce the noise in the above figure, the general observation of similarity would remain the same. Table 3.9 below shows the resulting indices per case.

Table 3.9 Reliability Index Results Considering Combinations of Load and Soil Randomness

	Sources of Randomness		
Soil Case Type	Soil	Loading	Soil & Loading
Independent Variation	4.6	-	3.0
Perfect Correlation	3.8	-	2.8
No Randomness	-	4.1	-

Unsurprisingly, taking into account randomness in both soil and loading conditions reduces β.

3.3 Conclusions

The main objective of this chapter was to determine the effect of soil properties on structural response. The serviceability requirements (defined by horizontal pile head displacement and pile head rotation) provided succinct deformation-based limit states that were conducive to reliability analysis. First-order estimates of the reliability index β were dominated by pile head rotation and thus the probability of horizontal pile head displacement failure was considered negligible.

Analyses were performed to determine the sensitivity of β to various parameters. Considering relative density to be a function of friction angle (φ'), epistemic soil randomness was modeled with the limiting correlation cases of perfect vertical spatial correlation and independent variation

(characterized by beta distributions). Using 10,000 samples to estimate the mean and standard deviation of the safety margin, β was calculated using a first order method (see Equations 3.7 and 3.8).

Several conclusions were made from these analyses:

- Assuming perfectly correlated soil properties yielded consistently lower β values than assuming independent variation due to variation in pile head response.
- As the COV of a symmetric φ' distribution increases, β decreases nonlinearly.
- Pile head rotation α increased with the COV of a symmetric φ' distribution, illustrating the nonlinear aspects of soil-structure interaction.
- If the COV of φ' is assumed constant at 5%, β increases linearly with mean friction angle, $\mu_{\varphi'}$

In realistic design situations, a site investigation is performed at a desired location and the pile foundation is designed according to available soil properties. Consequently, examining the effect of soil variation on β does not appropriately illustrate the problem from the designer's viewpoint. Given an assumed soil profile (where φ' was characterized by a beta distribution with $\mu_{\varphi'}$=35° and COV = 5%), the sensitivity of β to pile design parameters was assessed. A contour plot comparing constant values of β and moment of inertia (Figures 3.20 and 3.21) revealed that the bending capacity of the pile was the most influential pile parameter. When β was analyzed over a range of embedment depths, the index value converged at approximately 38 m for the Lesny, Paikowsky & Gurbuz (2007) example.

Similar to soil variation and pile design parameters, a preliminary sensitivity analysis was performed for variation in loading conditions. In MATLAB simulations, gravity loads were considered deterministic while the horizontal loads and overturning moment were modeled as random and perfectly correlated. The loading values given by Lesny, Paikowsky & Gurbuz

(2007) were assumed to be mean values and load variation was characterized by a Weibull distribution with COV 5% (to mimic the soil variation studies). Comparing the results of the convergence studies of both soil and load variation (Figure 3.24), it was determined that β is similarly sensitive to load variation as soil variation.

When 5% COV was considered for both load and soil randomness, β decreased to 2.8 with the limiting case of perfect correlation. Despite the reduction in β, the COV for 20 estimations of β was similar to the cases of only load or soil randomness. A more rigorous study of load variation would include site-specific wind and wave data.

This chapter concludes the sensitivity studies for typical OWT pile foundations.

CHAPTER 4

LARGE DIAMETER EFFECTS

When the API equations are extrapolated for OWT pile foundations, theoretical research has shown that the strength of piles is overestimated for pile diameters exceeding 2 m (Wiemann, Lesny, & Richwien, 2004). Comparing the analysis results of finite element models to the API *p-y* method, Wiemann, Lesny & Richwien (2004) suggest an adjustment factor for the initial modulus of subgrade

$$k^*(b) = k\left(\frac{b_{ref}}{b}\right)^{\frac{4(1-a)}{4+a}} \quad \textbf{(4.1)}$$

Where b_{ref} is the diameter of a reference pile of 1-2 m and a is 0.6 for medium-dense cohesionless soils or 0.5 for dense cohesionless soils.

The API method has been considered applicable for pile diameters up to 2 m in diameter, which is why the adjustment factor reduces the modulus of subgrade based on the relationship of the designed pile diameter to a reference pile of 1-2 m.

Since there are no particular recommendations regarding what dimension the reference pile diameter should be, a brief analysis was conducted to examine the behavior of the reliability index (β) with regard to the choice of reference pile diameter (see Figure 4.1). For this analysis, the pile parameters and load values given by Lesny, Paikowsky & Gurbuz (2007) were assumed to be deterministic values and φ' was characterized by a beta distribution with $\mu_{\varphi'}$ = 35° and 5% COV.

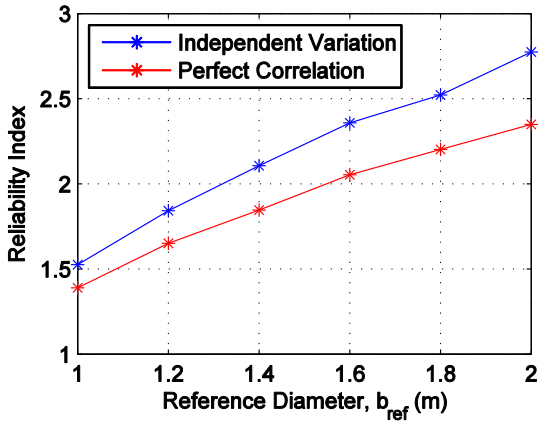

Figure 4.1 Reliability Index vs. Reference Diameter

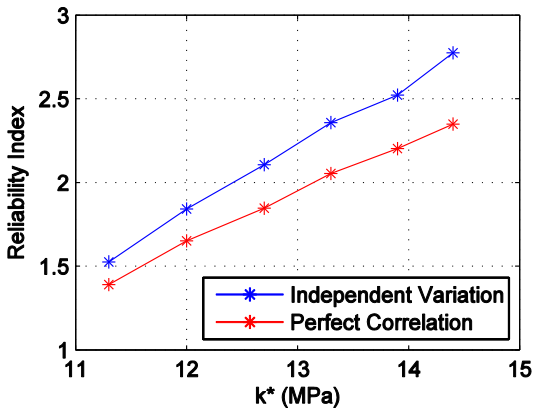

Figure 4.2 Reliability Index vs. Adjusted Initial Modulus of Subgrade (k*)

In Figure 4.1, β demonstrates linearly increasing behavior as b_{ref} increases. If k* is utilized in design, any choice of b_{ref} decreases β to 1.4-2.8 (depending on b_{ref} and soil variation case) from the previously calculated range of 3.8-4.6 (representing the limiting cases of perfect correlation and independent variation, respectively). The linearly increase in β shown in Figure 4.2 and its similarity to Figure 4.1 clearly demonstrates the linear relationship between k* and b_{ref}, which can be seen algebraically in Equation 4.1.

Considering the design life of an OWT, the target β is 4; however, the target for a 1-year return period is 1.5 (Stuyts, Vissers, Cathie, & Jaeck, 2011; Phoon, 2008). It is unclear which target β should be applied to this scenario, given that 50-year return periods are used for loading conditions and serviceability limits are used as a reference for pile head limit state.

4.1 Conclusions

The large diameter-adjusted k* suggested by Wiemann, Lesny & Richwien (2004) reduces the stiffness of piles by approximately 50-70%, depending on the choice of $b_{ref.}$ Consequently, k* also reduces β somewhat substantially. No full-scale tests have been performed to confirm these

results, but various researchers have concurred using finite element modeling that the API method is insufficient for designing piles with diameters in excess of 2 m (Wiemann, Lesny, & Richwien, 2004; Abdel-Rahman & Achmus, 2005). Current design standards do not include any changes to take into account large-diameter effects.

CHAPTER 5

NATURAL FREQUENCY ANALYSIS

Multiple influences must be considered during the dynamic design of OWTs: the frequency spectra of wind loading, wave loading, and mechanical frequency intervals. Once these input spectra are determined, a natural frequency is selected and an iterative design methodology is used to ensure that the foundation and the support structure of the OWT are adequately removed from a resonant range. In Figure 5.1 below, the frequencies to avoid are demonstrated graphically for the NREL 5MW Reference Turbine (Petersen, et al., 2010).

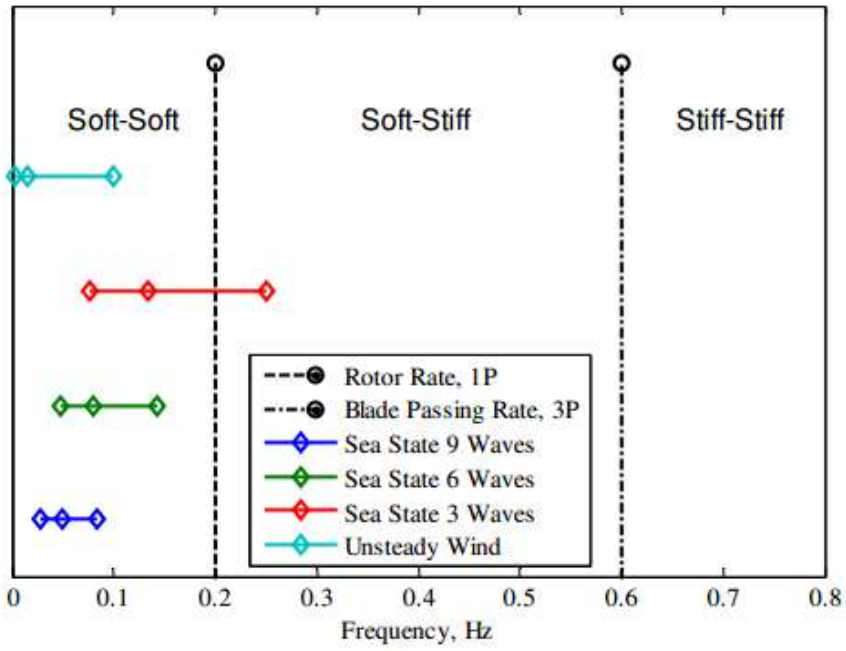

Figure 5.1 Structural Design Regime for Offshore Wind Turbines (Petersen, et al., 2010)

Three sea state wave distributions are depicted in Figure 5.1. These sea states are determined by the mean wind speed, the fetch (the distance over which the wind blows), and the duration of the

wind over the open water (NASA, 2000). A sea state is generally described by significant wave height, which is the average height of the one-third highest waves (NASA, 2000).

The frequencies 1P and 3P represent the mechanical excitation caused by the rotation of one rotor blade and the combination of all three rotor blades, respectively. OWTs can be designed according to three different regimes: if f_1 is designed to fall below both the 1P and 3P frequencies, the design is considered "soft-soft"; similarly, if it is designed to fall above both fundamental frequencies, the design is "stiff-stiff" and in between would be "soft-stiff" (Petersen, et al., 2010). The majority of OWTs are designed to be soft-stiff (LeBlanc, Houlsby, & Byrne, 2010).

This chapter focuses on solving the characteristic eigenvalue problem for natural frequency. A deterministic model is developed initially and validated by the published natural frequency values for the NREL 5MW Reference Turbine. The published model of the NREL 5MW Reference Turbine is for an onshore design; the substructure and pile are added to the model to determine the necessary adjustments in wall thickness that would be required to maintain the same first natural frequency as the Reference Turbine.

After the support structure and foundation wall thicknesses are determined, randomness is included in the eigenvalue problem. With the inclusion of soil variability, randomness is introduced into the stiffness matrix, resulting in a distribution of potential frequencies that may occur.

Moving from a static to dynamic analysis, *p-y* curves were reduced by 10% per API for cyclic loading. The effects of damping will be neglected.

5.1 Deterministic Eigenvalue Problem

The deterministic eigenvalue problem (Equation 5.1) assumes all input variables are known, non-random quantities where $\boldsymbol{K}$ is the global stiffness matrix, $\boldsymbol{M}$ is the global mass matrix, and ω is the natural frequency (rad/s).

$$det(\boldsymbol{K} - \omega^2 \boldsymbol{M}) = 0 \tag{5.1}$$

Using MATLAB to solve the eigenvalue problem, it was assumed that the steel of the foundation and support structure is linear, as well as soil-pile resistance.

5.1.1 NREL 5MW Reference Turbine Validation

The model was developed in stages, focusing first on the tower of an onshore turbine, approximated by a large cantilever. The cantilevered tower was modeled using the properties listed in Table 5.1 from the NREL 5MW Reference OWT (Jonkman, Butterfield, Musial, & Scott, 2009).

Table 5.1 Tower and Transition Piece Properties

Property	Value
Tower Height	90 m
Tower Base Diameter & Wall Thickness	6 m, 0.035 m
Tower Top Diameter & Wall Thickness	3.87 m, 0.025 m
Modulus of Elasticity	210 GPa
Density of Steel	8,500 kg/m^3
Nacelle & Rotor Mass	350,000 kg
Tower Mass	347,460 kg

The radius and thickness of the tower were assumed to be linearly tapered from the tower base to tower top. The density of steel, typically considered 7,850 kg/m^3, was increased to 8,500 kg/m^3 to include paint, bolts, welds and flanges (Jonkman, Butterfield, Musial, & Scott, 2009).

For finite element modeling in MATLAB, a lumped mass matrix was used to model the mass distribution of the tower, where the element mass matrix (***m***) is defined per Equation 5.2.

$$m = \frac{\rho AL}{24}\begin{bmatrix} 12 & 0 & 0 & 0 & 0 & 0 \\ 0 & 12 & 0 & 0 & 0 & 0 \\ 0 & 0 & L^2 & 0 & 0 & 0 \\ 0 & 0 & 0 & 12 & 0 & 0 \\ 0 & 0 & 0 & 0 & 12 & 0 \\ 0 & 0 & 0 & 0 & 0 & L^2 \end{bmatrix} \quad \textbf{(5.2)}$$

where ρ (kg/m^3) is the mass density, A is the cross-sectional area (m^2), and L is the length of the element (m).

The lumped mass matrix distributes inertial mass to each degree of freedom (DOF) on the diagonal (see Eq. 5.2 and Figure 5.2) to preserve linear momentum (e.g., the sum of the mass distributed in the *u*-direction is equal to the element mass).

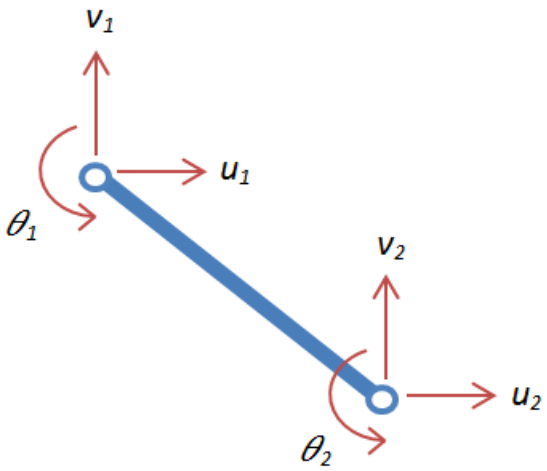

Figure 5.2 Example Finite Element with Illustrated DOFs

The lumped mass matrix is advantageous not only due to the ease of compilation but also because it reduces the computational time involved in the solution of the eigenvalue problem. The mass of the rotor hub and nacelle was added to u_1 and v_1 of the first element representing the top of the tower. Hub and nacelle mass was not distributed to the rotational degree of freedom θ_1 because it is fully affixed (and therefore not rotating about the tower).

The stiffness matrix $\boldsymbol{K}$ was formed in an identical manner to the quasi-static model's stiffness matrix, though initially the base of the tower was considered fully fixed (at sea level) and the effect of the sub-sea support structure was neglected.

A convergence study was performed to determine the appropriate element size for modeling the tower, using the third mode natural frequency (measured in Hz in Figure 5.3).

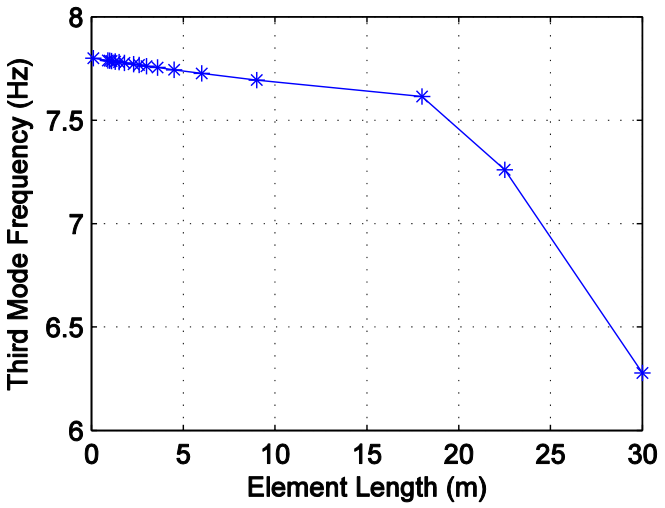

Figure 5.3 Convergence of Third Mode Frequency for NREL 5MW Reference Turbine

An element size of 6 m will be sufficient for modeling the NREL turbine tower.

The natural frequencies for the first three modes are listed in Table 5.2, using the 6 m element discretization. The tower mass calculated by the MATLAB model was 349,210 kg, which is only 0.5% more than the published value given for the NREL 5MW Reference Turbine.

Table 5.2 Dynamic Property Output for the NREL Reference Turbine

Mode	Natural Frequency (Hz)	Natural Frequency (rad/s)	Natural Period (s)
1	0.3162	1.987	3.163
2	2.881	18.10	0.3471
3	7.737	48.61	0.1292

Jonkman, Butterfield, Musial, & Scott (2009) list first mode frequencies ranging from 0.3120 to 0.3240 Hz considering the results fr006Fm FAST and ADAMS for fore-aft and side-to-side first mode behavior of the turbine. The MATLAB result above is within this range and varies from the average of the published values (0.3180 Hz) by less than 0.6%, validating the dynamic property output of the deterministic model.

5.1.2 **Deterministic Parametric Studies**

Given the results from Section 5.1.1, the NREL 5MW Reference Turbine model developed in MATLAB can be adapted to include the substructure and foundation (see Figure 5.4).

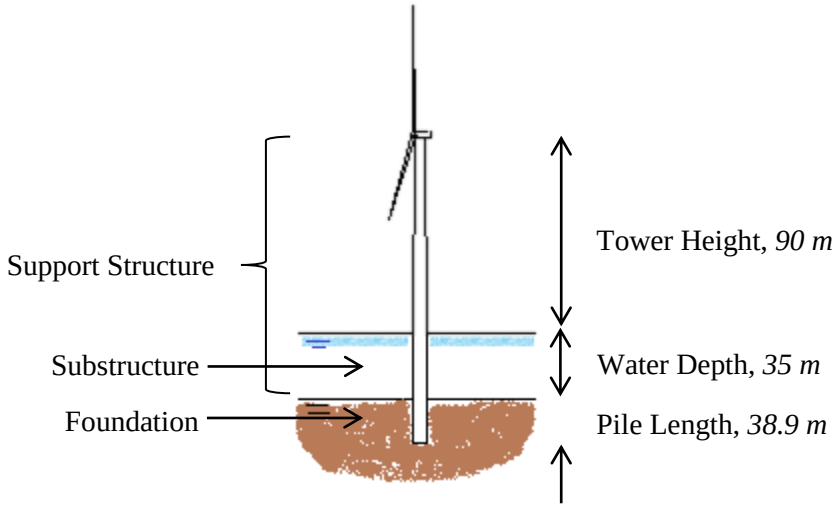

Figure 5.4 Dimensions of NREL 5MW Reference Turbine in North Sea Conditions

Keeping with the parametric studies of Chapter 3, the substructure was added, with a length equivalent to the mean water depth listed by Lesny, Paikowsky & Gurbuz (2007) of 35.0 m. The accepted depths for monopile foundations are typically up to 30 m, though some have argued that they can be used for depths up to 50 m (Lesny & Hinz, 2007; Malhotra, 2010).

The damping effects of water were neglected and the wall thickness of the substructure was assumed to be constant and equal to the wall thickness at the base of the tower.

Similar to the convergence study for the tower, a study was performed to determine the appropriate element size for the substructure using the 6 m elements for the tower as previously determined in Section 5.1.1 (see Figure 5.5).

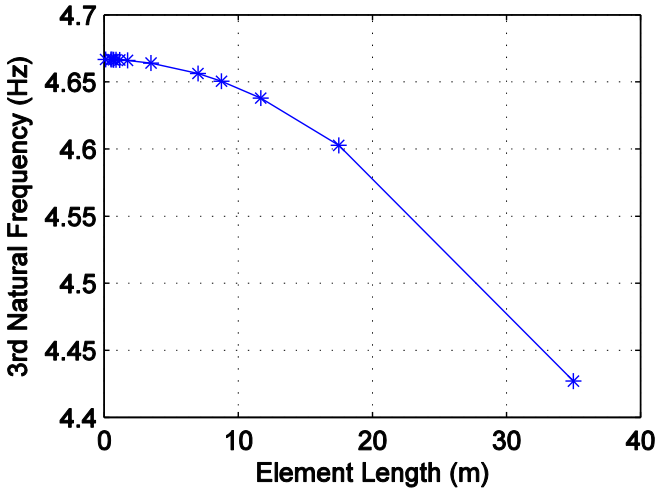

Figure 5.5 Convergence of Third Mode Natural Frequency for NREL 5MW Reference Turbine, Including Transition Piece

Three 11.67-m elements were chosen to model the substructure. The added height from the substructure increased the height of the "on shore" turbine to 125 m, decreasing the natural frequency to 0.2132 Hz.

In the design of the NREL 5MW Reference Turbine, the engineers chose to increase the wall thicknesses of 0.027 and 0.019 m for the tower base and top (respectively) by 30% in order to maintain a soft-stiff design regime (Jonkman, Butterfield, Musial, & Scott, 2009). Using a similar methodology to compare the effects of wall thickness on natural frequency, parametric studies were performed using percentage increases of the NREL tower wall thickness dimensions and various substructure wall thicknesses (see Figure 5.6).

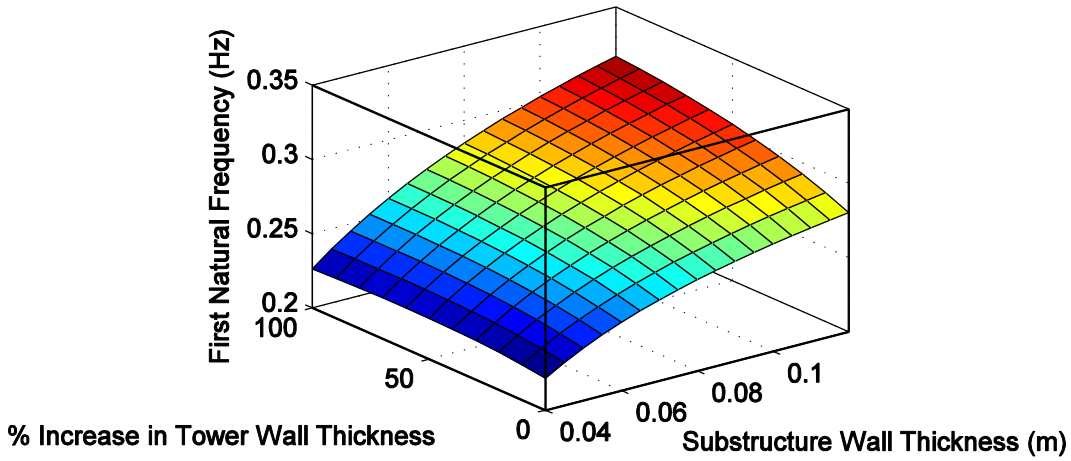

Figure 5.6 Effect of Wall Thickness on Natural Frequency, Considering Tower and Substructure

In order to bring the first natural frequency (f_1) back up to the minimum 0.3120 Hz, Figure 5.7 shows that the substructure wall thickness would need to be larger than 0.110 m and the tower wall thickness would need to increase by 70% or more.

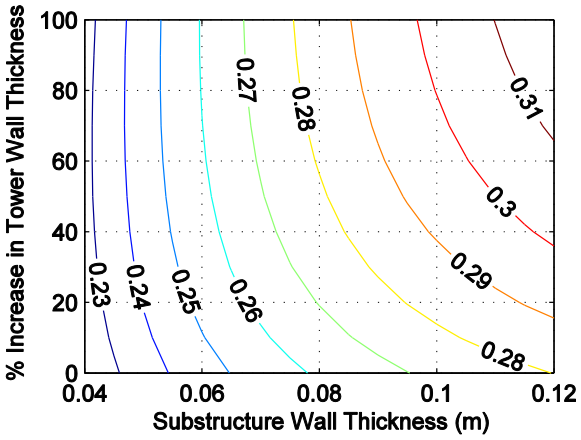

Figure 5.7 Natural Frequency Contour Plot, in Reference to Support Structure Wall Thickness

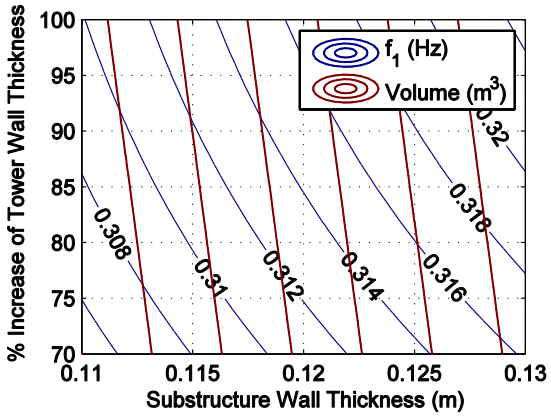

Figure 5.8 Comparison of Support Structure Volume and Natural Frequency Contours

To optimize the choice of wall thicknesses, the contour plot of f_1 from Figure 5.7 was expanded and compared to contours of constant support structure volume (see Figure 5.8). The volume contours (using average, mid-height tower properties) indicate that substructure wall thickness takes precedence over the percentage increase of tower properties. If the substructure wall thickness is considered to be 0.113 m, a 100% increase is required of the tower wall thicknesses to be within the range of f_1 listed for the NREL 5MW Reference Turbine (see Table 5.3).

Table 5.3 Support Structure Wall Thicknesses, Considering Soil-Level Fixity

Property	Value
Substructure Wall Thickness	0.113 m
Tower Base Wall Thickness	0.070 m
Tower Top Wall Thickness	0.049 m

With the properties and discretization of the support structure established, a convergence study regarding the monopile and soil springs was conducted. The pile is assumed to have the same diameter and wall thickness as the substructure. Pile properties incorporate the mass of the soil inside of the pile.

In Figure 5.9 below, soil springs were considered to have infinite stiffness.

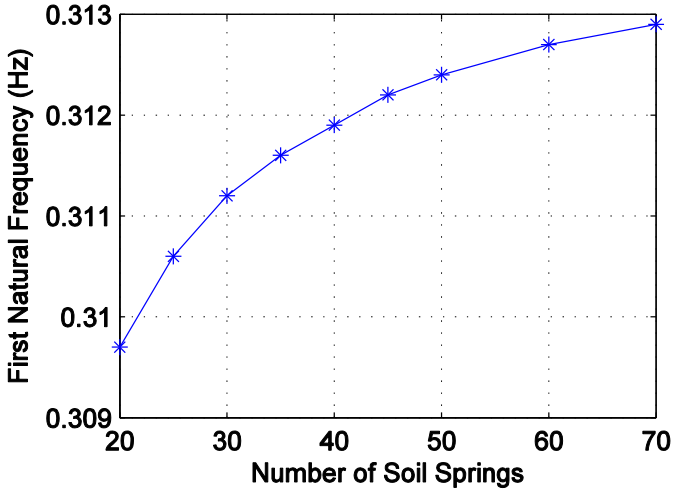

Figure 5.9 Convergence of First Natural Frequency with Regard to Infinitely Stiff Soil Springs

Per expectation, as the number of infinitely stiff springs increase, so does f_1. Using 0.3120 Hz as the target value, 40 infinitely stiff soil springs (spaced approximately 1 m apart) are necessary to equate a model including the pile foundation to fixity below the substructure. A convergence study including real soil stiffness with constant $\varphi' = 35°$ can be seen below in Figure 5.10.

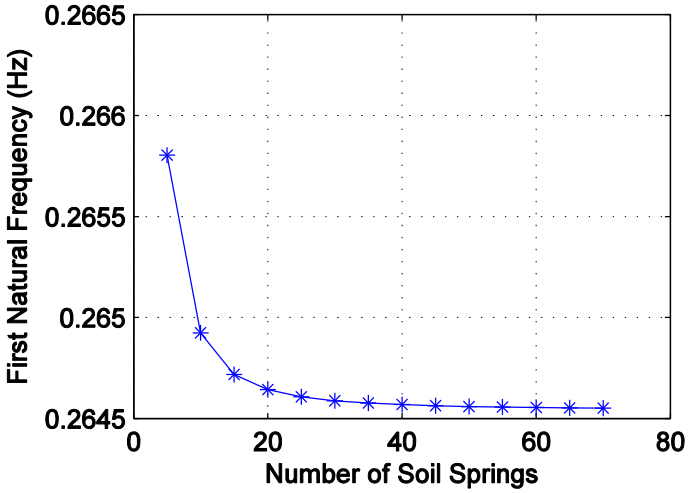

Figure 5.10 Convergence of First Natural Frequency with Respect to Soil Springs

According to Figure 5.10, f_1 converges quickly; using just 5 soil springs is still less than 0.5% different than the converged value of 0.2646 Hz. Given the results from the reliability analysis of Chapter 3 however, 20 soil springs will be used to model the pile.

Because the converged value of f_1 represents a 15% decrease in stiffness from the NREL 5MW Reference Turbine, the substructure and tower wall thicknesses were again increased to target the minimum 0.3120 Hz.

Figures 5.11 and 5.12 below illustrate the effect of substructure wall thickness and percentage increase of tower wall thickness on f_1.

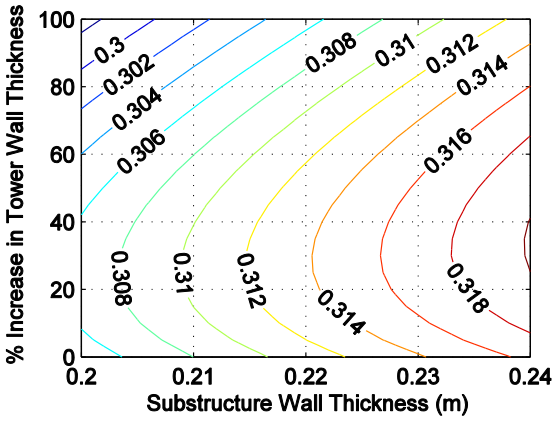

Figure 5.11 Natural Frequency Contour Plot with Respect to Wall Thickness, Including Monopile Foundation

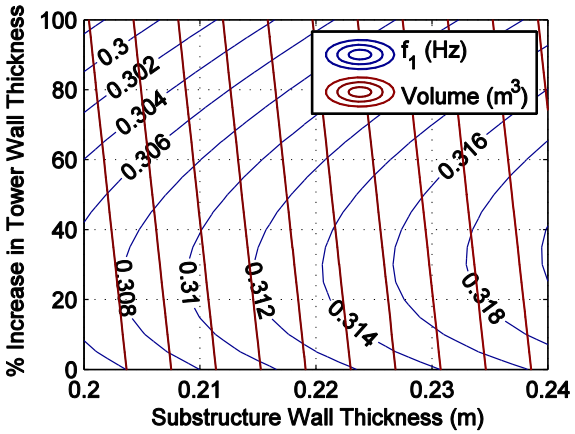

Figure 5.12 Comparison of Volume and Natural Frequency Contours of Support Structure and Monopile Foundation

While larger wall thickness does increase stiffness, it also adds more mass to the system. At a certain point, the structural advantage of increasing wall thickness is decreased by the additional mass, which is demonstrated by the peak in contour curves of Figure 5.12. Using the minimum volume of steel as the optimum point, the peak of the 0.3120 Hz curve is at a transition wall thickness of approximately 0.215 m and 30% increase would both increase f_1 while minimizing the amount of steel used. The new wall thickness properties can be found below in Table 5.4.

Table 5.4 Support Structure and Foundation Wall Thicknesses

Property	Value	% Increase from Soil Fixity Model
Pile & Substructure Wall Thickness	0.215 m	53%
Tower Base Wall Thickness	0.091 m	30%
Tower Top Wall Thickness	0.064 m	30%

Using the same soil spring discretization of approximately 2 m, f_3 is not effectively changed by embedment length (see Figure 5.13).

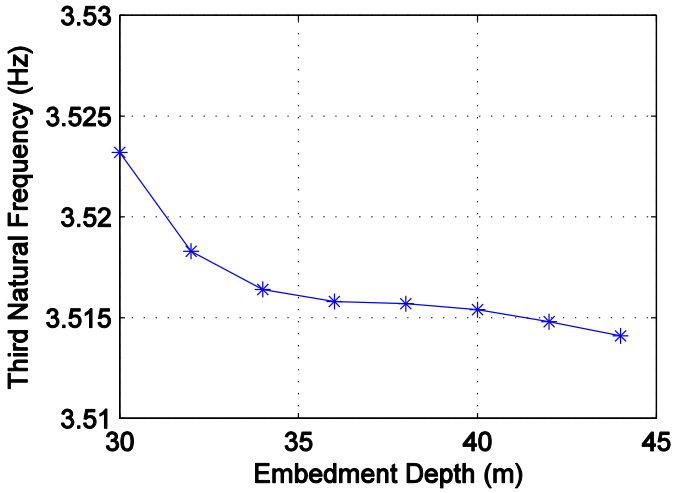

Figure 5.13 Effect of Embedment Depth on Third Natural Frequency

While a slight decrease in f_3 can be noted from 30 m of embedment to nearly 45 m of embedment, the change in frequency is negligible – less than 0.3%. This figure confirms that frequency has converged for a pile embedment depth of 38.9, per Lesny, Paikowsky, & Gurbuz (2007).

The natural frequencies for the first three modes of the NREL 5MW Reference Turbine MATLAB model (and subsequent two evolutions) are listed in Table 5.5.

Table 5.5 Comparison of Unadjusted Dynamic Property Output for the NREL 5MW Reference Turbine, Including Substructure and Monopile Foundation

Mode	Natural Frequency (Hz)		
	Tower Only	Support Structure (Tower & Substructure)	Support Structure & Pile
1	0.3162	0.2132	0.1841
2	2.881	1.560	1.275
3	7.737	4.638	3.776
Avg. % Decrease from Tower Only:		*39%*	*50%*

Without increasing the wall thickness from the original NREL parameters, f_1 would be reduced by 50%.

If we use this model to compare the effect of φ' on f_1, Figure 5.14 illustrates that f_1 increases nonlinearly with φ' for the range of medium dense sand. The difference between the minimum f_1 of 0.3120 and the maximum 0.3186 Hz is 5%.

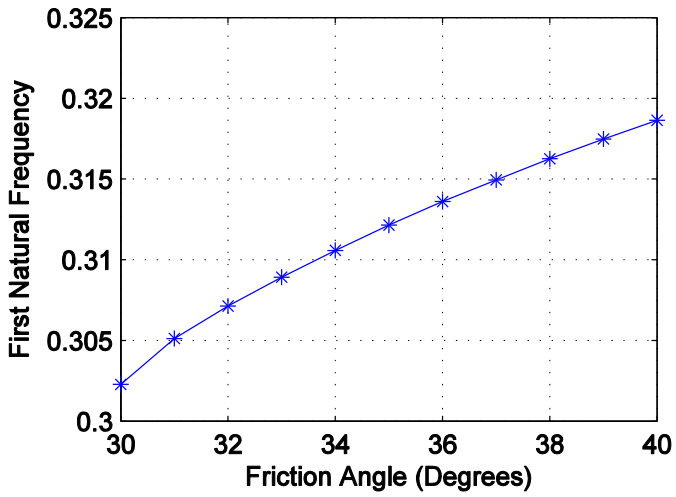

Figure 5.14 First Natural Frequency vs. Friction Angle

5.2 Random Eigenvalue Problem

Randomness in soil properties can now be taken into account to produce a distribution of frequencies that may occur. Including soil variability introduces randomness in the stiffness matrix portion of the eigenvalue problem, while the mass remains deterministic.

In natural frequency design of OWTs, it is important that the 1P and 3P frequencies associated with the fundamental frequencies of one and three rotors rotating (respectively, for a three-bladed turbine) are avoided. In addition to mechanical vibrations, dynamic excitation from wind and waves frequency spectra must be taken into account as well.

Rather than producing a single value for the frequency associated with each mode, a random **K** matrix will produce a distribution of f_1; comparing this distribution to the excitation spectra in Figure 5.1, the probability of resonance can be determined.

As in Chapter 3 regarding pile foundation reliability, both cases of independent variation and perfect correlation were considered in terms of vertical variability of the soil property φ'. Distribution of φ' was considered to be symmetric with $\mu_{\varphi'}$ = 35° and 5% COV. Using MC simulation to produce estimates of f_1, σ_{f1} converges at approximately 150 samples for both cases (see Figure 5.15).

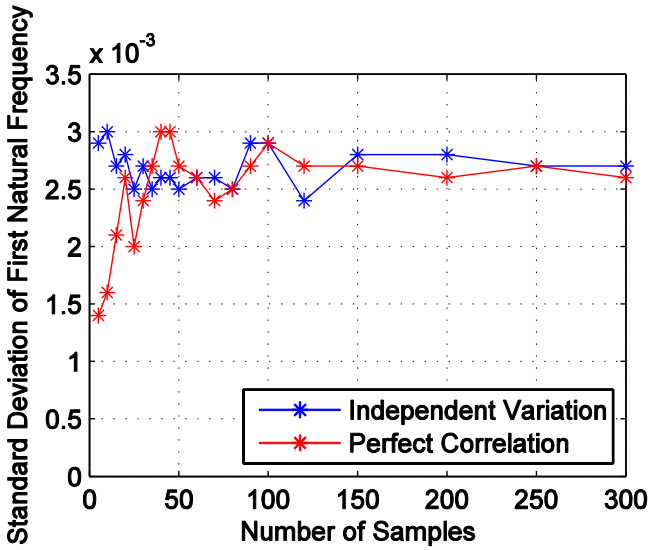

Figure 5.15 Convergence of Standard Deviation of First Natural Frequency

When estimating f_1, the difference between using independent variation or perfect correlation to model soil variation is small. The similarity between these distributions can be seen in the outlines of histograms as seen below in Figure 5.16, using 1000 samples to increase the definition.

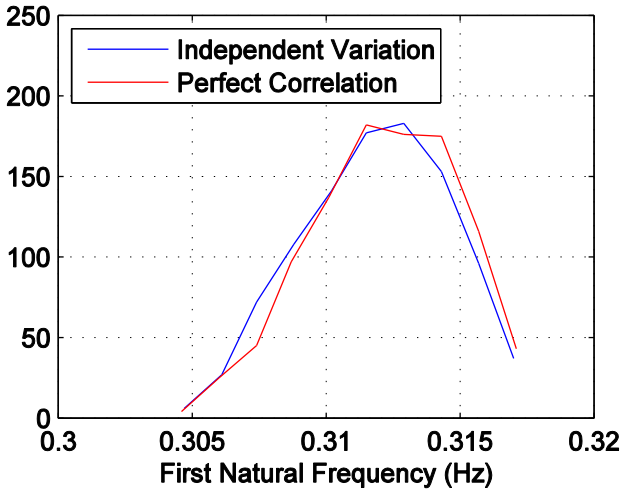

Figure 5.16 First Natural Frequency Distribution Comparison of Soil Variation Cases, 1000 Samples

The results of the two cases are compared in Table 5.6.

Table 5.6 Frequency Distribution Comparison of Soil Variation Cases

	Minimum	Maximum	μ_{f1}	σ_{f1}
Independent Variation	0.3040	0.3177	0.3118	2.715×10^{-3}
Perfect Correlation	0.3039	0.3178	0.3122	0.0027

The COV of f_1 for both of these cases is less than 0.9%. This is unsurprising, as pile foundations are designed to provide full fixity to the OWT. Less than 28% of these distributions fall outside of a $\pm$1% change in natural frequency, indicating that while the variation in f_1 is small, it is not small enough to be considered negligible.

With the 1P and 3P frequencies for the NREL 5MW Reference Turbine expanded into bands (capturing the effect of variable speed rotors), there is no overlap between the frequency distribution and the given excitation spectra (see Figure 5.17).

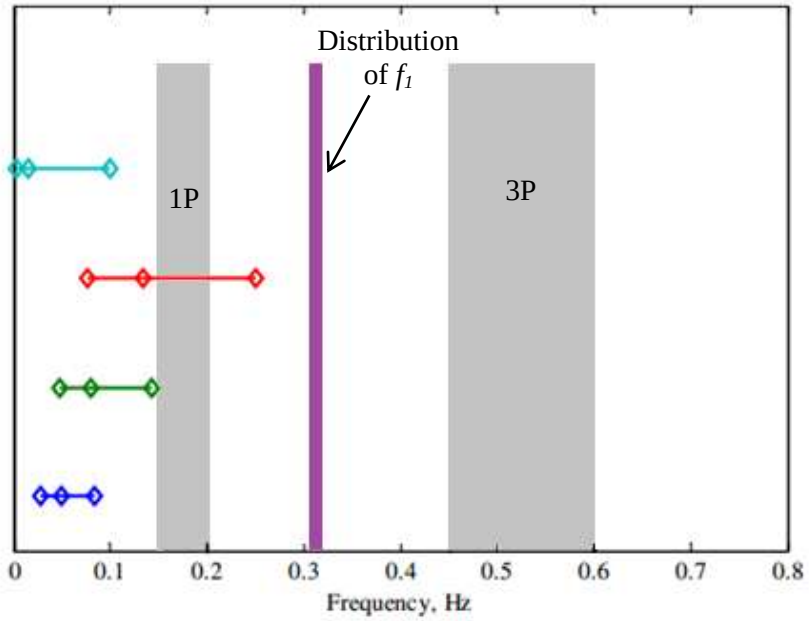

Figure 5.17 Offshore Wind Turbine Frequency Compared to Excitation Frequencies (Petersen, et al., 2010)

This means that the probability of resonance failure for this OWT turbine design is negligible.

5.3 Conclusions

A natural frequency analysis of the NREL 5MW Reference turbine described by Jonkman, Butterfield, Musial, & Scott (2009) was performed in MATLAB by solving the characteristic eigenvalue problem. The resulting first natural frequency (f_1) agreed with the FAST and ADAMS results published, validating the MATLAB modeling process.

The Reference Turbine was based on the design of an onshore wind turbine and thus neglected any portion of the OWT below the water surface (substructure and foundation). In a deterministic analysis, the substructure and then pile foundation were added to the MATLAB model, increasing wall thickness to maintain f_1 of 0.3120 Hz (the minimum frequency listed by Jonkman, Butterfield, Musial & Scott (2009)). Damping and water effects were neglected. The progression of wall thickness increase can be seen in Table 5.7 below.

Table 5.7 Summary of Wall Thickness Increases

	NREL 5MW Reference	Tower & Substructure	Tower, Substructure & Pile
Tower (Bottom/Top)	0.025 / 0.035 m	0.049 / 0.070 m	0.064 / 0.091 m
Substructure & Pile	-	0.113 m	0.215 m

Tower wall thickness had to be increased by a factor of nearly 2.6 to maintain the minimum published frequency by Jonkman, Butterfield, Musial & Scott (2009).

As in Chapters 3 and 4, soil property variability was taken into account by modeling vertical friction angle (φ') variation. The difference in f_1 distribution between independently varying and perfectly correlated soil properties was negligible (see Figure 5.16). The COV of both f_1

distributions was less than 0.9%. Despite this small variation, nearly 28% of the distributions fell outside of $\pm 1\%\ \mu_{f1}$, indicating that the effect of soil variability should probably not be neglected.

When the full range of f_1 was overlaid on the frequency diagram by Petersen et al. (2010), there was no overlap with the 1P, 3P, wind or wave frequencies, rendering the probability of resonance failure as negligible.

CHAPTER 6

CONCLUSIONS AND RECOMMENDATIONS

Current design standards for offshore wind turbines (OWTs) utilize a deterministic design procedure that applies partial safety factors to take into account randomness in wind and wave loading. The goal of this thesis was to analyze the reliability of OWTs with monopile foundations using probabilistic methods.

Monopile foundations are the most popular design for OWT foundations due to the ease of design and load application. All standards use the API *p-y* method to design pile foundations in sand, which characterizes soil-pile resistance as a series of nonlinear springs along the length of the pile. Based on research performed by Reese et al. (1975) on 0.6 m-diameter piles, researchers have noted that there are significant drawbacks when the API *p-y* method is applied to OWT pile foundations exceeding 2 m in diameter. Moreover, there is limited understanding of soil-structure interaction for pile foundations under cyclic conditions; to account for cyclic loading, API RP2A reduces *p-y* curves by 10%.

Based on the published results of Lesny, Paikowsky & Gurbuz (2007), a static two-dimensional model of an OWT monopile foundation was created and validated using MATLAB. With this base model, epistemic randomness in soil properties was introduced by vertically varying friction angle (φ'). Relative density was related to φ' based on the figures from API and all soil properties were considered a function of φ'. Because the beta distribution can be banded above and below, it was used to model φ' within the range of medium dense sands (30°-40°). Without specific soil information from a site, the limiting cases for correlation of φ' (independent variation and perfect correlation) between soil springs were considered for all parametric studies.

A first order method was implemented to determine the reliability index (β) of the MATLAB model, using the serviceability limits of the pile head (in terms of displacement and rotation) to create safety margins. According to Stuyts et al. (2011), the target β for serviceability conditions is 1.5. For an ultimate limit state, Phoon (2008) recommended a β of 4. Rotation dominated β, and the contribution of failure probability from displacement was neglected. Throughout the soil-pile interaction studies, assuming perfectly correlated soil properties yielded lower values of β than assuming independently varying properties.

Regarding the effect of distribution properties, it was determined that as the COV of a symmetric (mean friction angle $\mu_{\varphi'}$ = 35°) φ' distribution increases, β decreases nonlinearly. If the COV of φ' is considered to be the maximum of 5% per Lacasse & Nadim (1996), β increased linearly with $\mu_{\varphi'}$.

Considering that realistic pile design situations are conducted with a given set of soil properties, the effect of pile diameter, wall thickness, and embedment depth on β were studied. In a parametric study, it was determined that the bending capacity of the pile directly influenced β, rendering the effect of pile diameter on API *p-y* curves negligible by comparison.

In a reliability analysis regarding embedment depth, the pile properties selected by Lesny, Paikowsky & Gurbuz (2007) were used and analyzed over a range of embedment depths. Reliability converged around 36 m, which agreed with the designed embedment depth of 38.9 m.

The wind and wave loads acting on OWTs are random. In a preliminary load sensitivity study, the quasi-static lateral load values from Lesny, Paikowsky, & Gurbuz (2007) were treated as mean values of Weibull distributions with 5% COV. A more realistic model would include site-specific

wind and wave data, from which the applied horizontal load and overturning moment would be derived.

Comparing the effects of random soil properties and mean load to mean soil properties and random load, β was more sensitive to load variation than soil variation. Considering randomness in both, the limiting values of β was 2.8; however, this study combined 50-year return periods for loading with serviceability limits which are traditionally associated with a return period of 1 year (Stuyts, et al., 2011).

The results did not include the effect of large pile diameters. Despite the fact that API *p-y* curves do not adequately capture soil-pile resistance for pile diameters beyond 2 m, no design standard has adopted the adjusted value k^* suggested by Wiemann, Lesny & Richwien (2004). If this adjustment value is incorporated, the limiting value of β can be reduced to 1.4.

A natural frequency analysis was conducted by solving the characteristic eigenvalue problem in MATLAB. Damping was neglected, soil was considered deterministic (φ' = 35°), and all materials were assumed to be linear. The NREL 5MW Reference Turbine was used to validate the MATLAB results, and the first natural frequency (f_1) agreed with the published results from FAST and ADAMS by Jonkman, Butterfield, Musial, & Scott (2009). The NREL 5MW Reference Turbine design did not include details regarding the substructure and pile foundation; consequently, when these parts of the OWT were added, f_1 decreased below the minimum published value of 3.120 Hz. Using the design methodology mentioned by Jonkman et. al (2009), the wall thicknesses were increased until f_1 agreed with the minimum value.

With the full dynamic OWT model designed, randomness was incorporated in the soil properties. Using the symmetrical beta distribution previously analyzed, φ' was assumed to vary vertically with $\mu_{\varphi'}$ of 35° and 5% COV. Interestingly, considering the limiting correlation cases of

independent variation and perfect correlation presented very little difference in the resulting distribution of f_1. The COV of f_1 was less than 0.9%, but using a $\pm$1% natural frequency cutoff as negligible, nearly 72% of the distribution was in the range of negligible variation. Though over a quarter of the frequencies landed beyond the negligible range, the band of frequencies did not overlap with the 1P and 3P frequencies of the NREL 5MW Reference Turbine. Additionally, the distribution of f_1 did not coincide with the assumed excitation frequencies from Sea State 3, 6, or 9 wave distributions or wind distribution.

While variation in soil properties did not majorly impact the results of the natural frequency analysis, it was evident that soil variation was a major influence in quasi-static reliability analyses. For future studies, a better metric for quantifying the impact of soil variation might include multiplying the frequency response function of the OWT by the loading spectra of wind and waves and then integrating for mean square response. Continued study of quasi-static reliability conditions would best include the results of an offshore soil site investigation, with which realistic soil properties and variation could be extracted and applied. Alternatively, it would also be useful to extend the range of soils considered to include all cohesionless and cohesive soil types.

Steel was considered a completely linear material in this thesis, and the potential for nonlinearity should be analyzed. Ideally, the issues associated with large diameter piles should also be monitored by comparing real-time wind and wave data to pile head displacement and rotation on an installed OWT. Several researchers have analyzed large diameter OWTs using finite element methods, but no results from large-scale testing or data from previously installed large-diameter OWTs has been published.

For further dynamic analysis, the effects of water on the substructure should be considered. Also, 1% damping should be included for the tower per Jonkman, Butterfield, Musial & Scott (2009). Large diameter adjustments were not made to the OWT monopile for the natural frequency analysis and should be taken into account for future studies.

While the simplicity of the monopile foundation option may be advantageous for design and analysis, this thesis illustrates the sensitivity of pile foundation reliability to soil conditions and large wall thicknesses required to avoid excitation frequencies. In order to assess the economic feasibility of monopile OWTs, design, construction, and installation cost estimations would be required for this design as well as estimations for other OWT foundation options.

BIBLIOGRAPHY

(2005). *LPILE Plus 5.0.* Austin, TX: Ensoft, Inc. Engineering Software.

Abdel-Rahman, K., & Achmus, M. (2005). *Finite Element Modelling of Horizontally Loaded Monopile Foundations for Offshore Wind Energy Converters in Germany.* University of Hannover, Germany, Institute of Soil Mechanics, Foundation Engineering and Waterpower Engineering. London: Taylor & Francis Group.

ABS. (2010). *Guide for Building and Classing Offshore Wind Turbine Installations.* Houston, TX: American Bureau of Shipping.

API. (2005). *Recommended Practice for Planning, Designing, and Constructing Fixed Offshore Platforms - Working Stress Design.* Washington, D.C.: American Petroleum Institute.

Ariston, I. K. (2010). *Grouted Connections for Offshore Wind Turbines.* TUDelft.

Baecher, G. B., & Christian, J. B. (2003). *Reliability and Statistics in Geotechnical Engineering.* John Wiley & Sons.

Bir, G., & Jonkman, J. (2008). Modal Dynamics of Large Wind Turbines with Different Support Structures. *ASME 27th International Conference on Offshore Mechanics and Arctic Engineering.* Estoril, Portugal: National Renewable Energy Laboratory.

Bolinger, M., & Wiser, R. (2008). *Annual Report on U.S. Wind Power Installation, Cost, and Performance Trends: 2007.* United States Department of Energy.

Bush, E., & Manuel, L. (2009). *Foundation Models for Offshore Wind Turbines.* Orlando, FL: American Institute of Aeronautics and Astronautics.

Cordle, A. (2006). *Final report for WP4.3: Enhancement of Design Methods and Standards.* Project UpWind.

Day, R. W. (2000). *Geotechnical Engineer's Portable Handbook.* New York: McGraw-Hill.

de Vries, W. E., & Krolis, V. D. (2004). *Effects of Deep Water on Monopile Support Structures for Offshore Wind Turbines.* Delft University of Technology, Duwind, Civil Engineering and Geosciences, Delft, the Netherlands.

DeGroot, D. J., & Baecher, G. B. (1993, January). Estimating Autocovariance of In-Situ Soil Properties. *Journal of Geotechnical Engineering, 119*(1).

Department of Energy. (2010). *20% Wind Energy by 2030.* United States Department of Energy.

DNV. (2009). *Offshore Standard DNV-OS-J101: Design of Offshore Wind Turbine Structures.* Norway: Det Norske Veritas.

Fenton, G. A., & Griffiths, D. V. (2000). Bearing Capacity of Spatially Random Soils. *8th ASCE Joint Specialty Conference on Probabilistic Mechanics and Structural Reliability.* Notre Dame, IN.

Gipe, P. (2006, June 7). *IEC Wind Turbine Classes*. Retrieved January 6, 2010, from Wind-Works: http://www.wind-works.org/articles/IECWindTurbineClasses.html

GL. (2005). *Guideline for the Certification of Offshore Wind Turbines.* Uetersen, Germany: Germanischer Lloyd WindEnergie GmbH.

Goldfingle, G. (2010, Spring). Wind Energy: Foundations. *European Foundations*, pp. 10-12.

Gur, T., Choi, J., Abadie, R. J., & Barrios, A. C. (2009). Assessment of Platform Cognac Using Instrumentation Data. *Offshore Technology Conference.* Houston, Texas.

Hamre, L., Khankandi, S. F., Strom, P., & Athanasiu, C. (2011). *Lateral Behaviour of Large Diameter Monopiles at Sheringham Shoal Wind Farm.* London: Taylor and Francis Group.

Houlsby, G. T., & Byrne, B. W. (2005, April). Design Procedures and Installation of Suction Caissons in Clay and Other Materials. *Geotechnical Engineering 158*(GE2), 75-82.

IEC 61400-3. (2009). *Design Requirements for Offshore Wind Turbines*. Internation Electrotechnical Commission.

Jonkman, J., Butterfield, S., Musial, W., & Scott, G. (2009). *Definition of a 5-MW Reference Wind Turbine for Offshore System Development.* Golden, CO: National Renewable Energy Laboratory.

Jonkman, J., van Dam, J., & Forsyth, T. (2003). Investigation of the IEC Safety Standard for Small Wind Turbine Design through Modeling and Testing. *ASME Wind Energy Symposium.* Reno, NV: National Renewable Energy Laboratory.

Kramer, S. L. (1988). *Development of P-Y Curves for Analysis of Laterally Loaded Piles in Western Washington.* Seattle, Wa: Washington State Department of Transportation.

Krolis, V. D., van der Tempel, J., & de Vries, W. (2007). *Evaluation of Foundation Design for Monopile Support Structures for Offshore Wind Turbines.* Delft University of Technology, Offshore Engineering, Delft, the Netherlands.

Lacasse, S., & Nadim, F. (1996). Uncertainties in Characterizing Soil Properties. *Uncertainty in the Geological Environment: From Theory to Practice* (pp. 49-75). Madison, WI: ASCE.

LeBlanc, C., Houlsby, G. T., & Byrne, B. W. (2010). Response of Stiff Piles in Sand to Long-Term Cyclic Lateral Loading. *Geotechnique, 2*(60), pp. 79-90.

Lesny, K., & Hinz, P. (2007). Investigation of Monopile Behavior under Cyclic Lateral Loading. *6th International Offshore Site Investigation and Geotechnics Conference*, (pp. 383-390). London.

Lesny, K., & Wiemann, J. (2005). *Finite-Element-Modelling of Large Diameter Monopiles for Offshore Wind Energy Converters.* Institute of Soil Mechanics and Foundation of Engineering. Essen, Germany: University of Duisburg-Essen.

Lesny, K., Paikowsky, S. G., & Gurbuz, A. (2007). Scale Effects in Lateral Load Response of Large Diameter Monopiles. *Geo-Denver.* Denver, CO: American Society of Civil Engineers.

Liu, C., & Evett, J. B. (2004). *Soils and Foundations* (6th ed.). Upper Saddle River, NJ: Pearson Prentice Hall.

Long, J. H., & Vanneste, G. (1994, January). Effects of Cyclic Lateral Loads on Piles in Sand. *Journal of Geotechnical Engineering, 120*(No. 1).

Malhotra, S. (2010, August). Supporting the Winds of Change. *Civil Engineering*, pp. 76-85.

Matlock, H. (1970). Correlations for Design of Laterally Loaded Piles in Soft Clay. *Offshore Technology Conference.* Dallas, TX.

Musial, W., & Ram, B. (September 2010). *Large-Scale Offshore Wind Power in the United States: Assessment of Opportunities and Barriers.* National Renewable Energy Laboratory.

NASA. (2000, August 11). *NASA-HDBK-1001.* National Aeronautics and Space Administration.

NREL. (2009, September 9). *Offshore Wind Turbine Foundations - Current & Future Prototypes*. Retrieved January 7, 2011, from OffshoreWind.net: http://offshorewind.net/Other_Pages/Turbine-Foundations.html

Petersen, B., Pollack, M., Connell, B., Greeley, D., Davis, D., Slavik, C., et al. (2010). *Evaluate the Effect of Turbine Period of Vibration Requirements on Structural Design Parameters: Technical Report of Findings.* Groton, CT: Applied Physical Sciences Corp.

Phoon, K.-K. (2008). *Reliability-based Design in Geotechnical Engineering: Computations and Applications.* New York, NY: Taylor and Francis.

Quarton, D. (2005). *An Internation Design Standard for Offshore Wind Turbines: IEC 61400-3.* Bristol, UK: Garrad Hassan and Partners, Ltd.

Rankine, K. J., Sivakugan, N., & Cowling, R. (2006). *Emplaced Geotechnical Characteristics of Hydraulic Fills in a Number of Australian Mines.* Springer.

Reese, L. C., Cox, W. R., & Koop, F. D. (1975). Field Testing and Analysis of Laterally Loaded Piles in Stiff Clay. *Offshore Technology Conference.* Dallas, TX.

Saue, M., Lanford, T. E., & Mortensen, N. (2011). Design of Monopile Foundations in Sand for Offshore Windfarms. *Frontiers in Offshore Geotechnics II* (pp. 611-616). Taylor & Francis Group.

Schafer, B. (2010). Personal Communication.

Sett, K., & Jeremic, B. (2009). Forward and Backward Probabilistic Simulations in Geotechnical Engineering. In M. Iskander, D. F. Laefer, & M. H. Hussein, *Geotechnical Special Publication No. 186: Contemporary Topics in In-Situ Testing, Analysis and Reliability of Foundations* (pp. 332-339). Orlando, FL.

Stancich, R. (2010, September 3). *Wind Energy Update*. Retrieved January 24, 2011, from What's New about Gravity Base Foundations for Offshore Wind?: http://social.windenergyupdate.com/qa/what%E2%80%99s-new-about-gravity-base-foundations-offshore-wind

Stuyts, B., Vissers, V., Cathie, D. N., & Jaeck, C. (2011). Optimizing Site Investigations and Pile Design for Wind Farms Using Geostatistical Methods: A Case Study. *Frontiers in Offshore Geotechnics II* (pp. 629-633). Taylor & Francis Group.

Thomsen, J. H., Forsberg, T., & Bittner, R. (2007). Offshore Wind Turbine Foundations - The COWI Experience. *26th International Conference on Offshore Mechanics and Arctic Engineering.* San Diego, CA: ASME.

Toft, H. S., & Sorensen, J. D. (2010). Reliability-Based Design of Wind Turbine Components. *TORQUE 2010: The Science of Making Torque from Wind*, (pp. 829-838). Crete, Greece.

Uzielli, M., Lacasse, S., Nadim, F., & Phoon, K. (2007). *Soil Variability Analysis for Geotechnical Practice.* London: Taylor & Francis Group.

Van Nostrand Reinhold. (2002). *Foundation Engineering Handbook* (2nd ed.). (H.-Y. Fang, Ed.) Norwell, MA: Kluwer Academic Publishers.

Wickremesinghe, D., & Campanella, R. G. (1993). Scale of fluctuation as a descriptor of soil variability. In Li, & Lo (Eds.). Balkema, Rotterdam: Probabilistic Methods in Geotechnical Engineering.

Wiemann, J., Lesny, K., & Richwien, W. (2004). *Evaluation of Pile Diameter Effects on Soil-Pile Stiffness.* University of Duisburg-Essen, Institute for Soil Mechanics and Foundation Engineering, Essen, Germany.